THE JOURNAL OF PHYSICAL CHEMISTRY LETTERS
A JOURNAL OF THE AMERICAN CHEMICAL SOCIETY

Open Access
This article is licensed under CC-BY-NC-ND 4.0

pubs.acs.org/JPCL
Perspective

A Reflection on the Use of Molecular Simulation to Respond to SARS-CoV-2 Pandemic Threats

Lorenzo Casalino, Carlos A. Ramos-Guzmán, Rommie E. Amaro,* Carlos Simmerling,* Alessio Lodola,* Adrian J. Mulholland,* Katarzyna Świderek,* and Vicent Moliner*

Cite This: J. Phys. Chem. Lett. 2025, 16, 3249−3263
Read Online
ACCESS | Metrics & More | Article Recommendations

ABSTRACT: Molecular simulations play important roles in understanding the lifecycle of the SARS-CoV-2 virus and contribute to the design and development of antiviral agents and diagnostic tests for COVID. Here, we discuss the insights that such simulations have provided and the challenges involved, focusing on the SARS-CoV-2 main protease (M^{pro}) and the spike glycoprotein. M^{pro} is the leading target for antivirals, while the spike glycoprotein is the target for vaccine design. Finally, we reflect on lessons from this pandemic for the simulation community. Data sharing initiatives and collaborations across the international research community contributed to advancing knowledge and should be built on to help in future pandemics and other global challenges such as antimicrobial resistance.

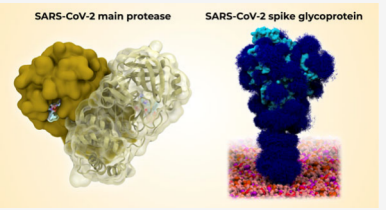

The appearance of the severe acute respiratory syndrome coronavirus-2 (SARS-CoV-2) in 2019 challenged scientists to understand molecular mechanisms in the viral life cycle and to contribute to developing compounds to block them. This task became even more complex due to rapid mutation of the virus. The COVID-19 pandemic brought scientists together[1] and inspired collective effort of the molecular modeling and simulation community to adopt a set of shared principles and commit to open science and data sharing in this space.[2] Here, we highlight some examples of the insight provided by different kinds of molecular simulations for two crucial SARS-CoV-2 targets: the main protease (M^{pro}/3CLpro, 3C-like protease), which is the target for antiviral drugs such as nirmatrelvir, and the spike protein, which is the target for vaccines. We also outline how collaborations between computational and experimental scientists enabled impactful discoveries.

A good example of a collaboration between computation and experiment was the COVID Moonshot Project: an open science, crowdsourced, structure-enabled drug lead discovery campaign that aimed to provide a roadmap for the development of new potential antivirals. This project built open knowledge bases, accelerating discovery efforts, and was a useful information-exchange hub, becoming an example of the potential effectiveness of open science antiviral discovery programs. The open science, patent-free nature of the project enabled many collaborators to provide in-kind support, including molecular simulations, synthesis, assays, and *in vitro* and *in vivo* experiments. By making all data immediately available and ensuring no need for materials transfer agreements, the research was accelerated globally along parallel tracks.[3]

Other initiatives emerged worldwide in which research groups started to work together (e.g., "*the Billion molecules against COVID-19 Challenge*") to tackle COVID-19.[4] The simulation community also benefited from the establishment of data repositories such as those set up by MolSSI and BioExcel,[5] and special allocation of computational resources by research funders and high performance computer centers, such as ARCHER and HECBioSim (EPSRC/UKRI), NSF, RIKEN (Japan), and the Spanish Supercomputing Network and the CINECA consortium, for computational projects devoted to this threat. These actions accelerated simulation work around the world, with consequent advances in knowledge and practical biomedical applications.[6]

Molecular simulations of various types (including multiscale methods)[7] can provide insight not readily available from experiments, such as on conformational fluctuations, allosteric binding, effects of glycosylation, and modeling chemical reaction mechanisms within proteins. We focus here in this brief review on two targets where molecular simulation has had a demonstrable impact: M^{pro}, which is the leading target for antivirals, and the spike glycoprotein, the target for vaccine design. Other reviews have focused on inhibitors targeting SARS-CoV-2 M^{pro}.[8] Even for just these two targets, we can cover here only a small fraction of published simulation work, and therefore, we highlight a few representative examples.

Received: December 22, 2024
Revised: February 19, 2025
Accepted: February 26, 2025
Published: March 21, 2025

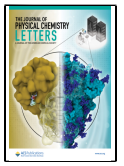

ACS Publications
© 2025 The Authors. Published by American Chemical Society

https://doi.org/10.1021/acs.jpclett.4c03654
J. Phys. Chem. Lett. 2025, 16, 3249−3263

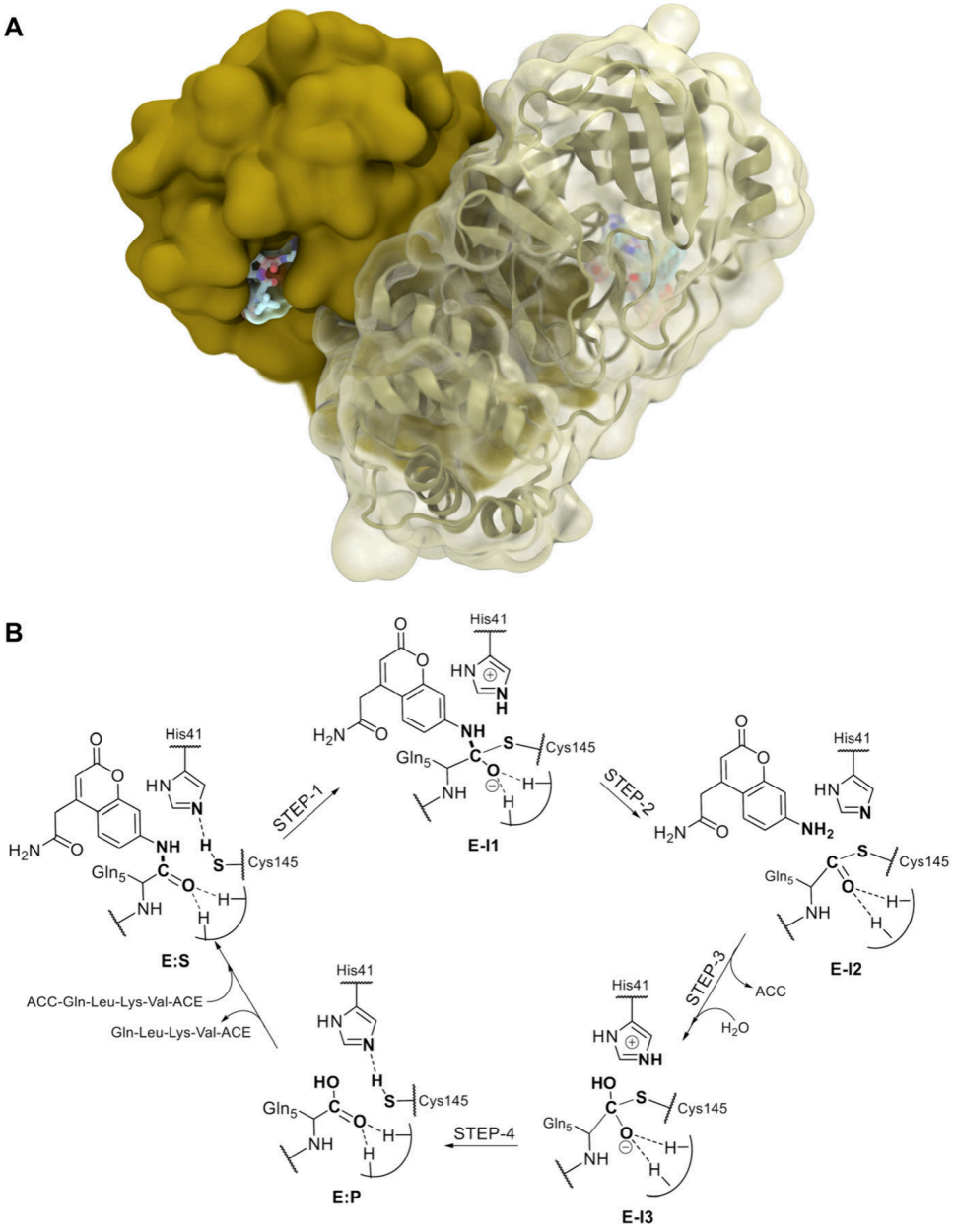

Figure 1. (A) Crystal structure of the SARS-CoV-2 M^{pro} dimer with nirmatrelvir docked in the active sites (PDB code 7TLL).[16] (B) Schematic representation of the molecular mechanism of the proteolysis of polypeptide Ac-Val-Lys-Leu-Gln-ACC (ACC is the 7-amino-4-carbamoylmethylcoumarin fluorescent tag) catalyzed by SARS-CoV-2 M^{pro} from QM/MM simulations. Figure 1B is reproduced with permission from ref 13, available under a CC-BY NC License. Copyright 2020 Royal Society of Chemistry.

SARS-CoV-2 MAIN PROTEASE (M^{PRO})

M^{pro} (also called 3CLpro) is a critical enzyme in the life cycle of the virus, essential for processing the polyproteins that are translated from the viral RNA.[9] As such, they are a prime target for antiviral drug development. M^{pro} is a cysteine protease with a catalytic dyad composed of Cys145 and His41, which is solvent-exposed and thus accessible to inhibitors. M^{pro} cleaves proteins directly after a glutamine residue, making it distinct from human proteases.[10] Mimicking this glutamine residue is a general strategy to inhibit M^{pro} selectively.

X-ray crystallography[10] showed that M^{pro} is formed of two identical protomers, each with a molecular mass of approximately 34 kDa (Figure 1A). Hydrogen bonds between the N terminal group of each monomer (N-finger) and the side chain of the C-terminal group of the peptide mimetics and inhibitors support the proposal that dimerization of the enzyme is necessary for optimal catalytic activity.[11] Neutron crystallography further shed light on how protonation states within the active-site cavity change upon inhibitor binding.[12]

Molecular simulations have played a crucial role in analyzing the *proteolysis reaction* of the SARS-CoV-2 M^{pro}. In early studies, researchers used quantum mechanics/molecular mechanics (QM/MM) enhanced sampling molecular dynamics (MD) simulations to simulate the reactions of a fluorescently tagged polypeptide,[13] because rate constants had been reported with this substrate.[14] Later, the proteolysis reaction was studied with the nonstructural protein (nsp)4/nsp5 peptide sequence from a viral polyprotein.[15] In the first study, the free energy surface was explored by using the semiempirical AM1 method to describe the QM region. This was followed by corrections of the AM1/

https://doi.org/10.1021/acs.jpclett.4c03654
J. Phys. Chem. Lett. 2025, 16, 3249−3263

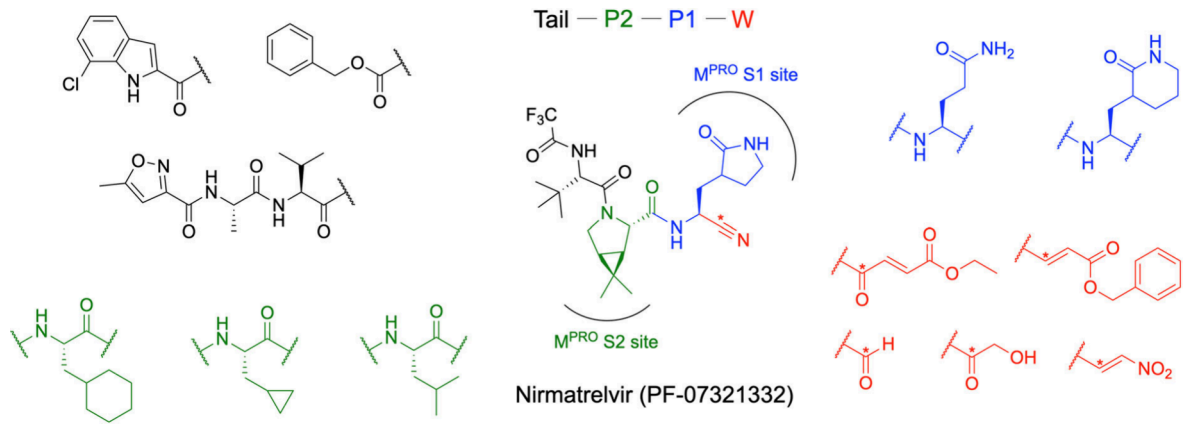

Figure 2. Classes of peptidomimetic fragments used to design covalent inhibitors of SARS-CoV-2 M^{pro}. The reactive center on the warhead (W) group is highlighted with an asterisk, red fragments. The P1 groups typically features a glutamine residue, or γ/δ-lactame bioisosteres, blue fragments. The P2 groups are moderate-size lipophilic, green fragments. The tail region, in black, is highly variable in size and shape, interacting with additional enzyme subpockets (i.e., S3 and S4, not shown). In the center is shown the chemical structure of nirmatrelvir, which incorporates pharmacophoric elements from earlier compounds, exemplifying the Tail-P2-P1-W structure. The S and P labeling corresponds to the Schechter and Berger nomenclature.[26]

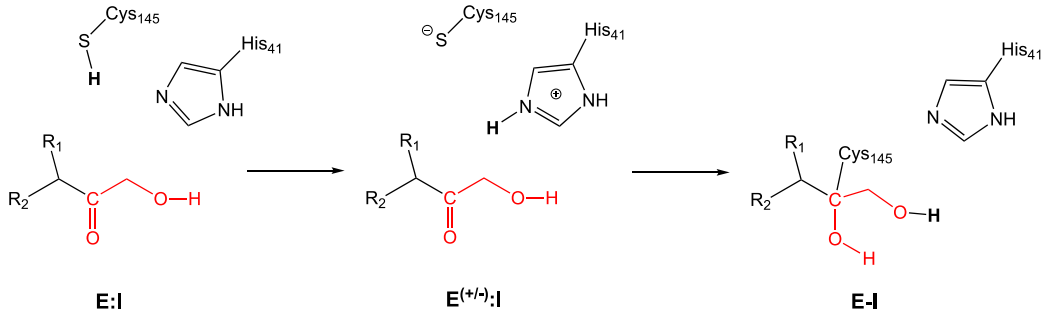

Figure 3. Schematic representation of the covalent inhibition mechanism of M^{pro} by a hydroxymethyl ketone inhibitor found from QM/MM simulations (compound B4 in ref 22).

MM free energy surface, as well as geometry optimization of stationary state structures at a higher density functional theory (DFT) level (M06-2X/MM). In the second study, the minimal free energy path was determined by using the adaptive string method (ASM), with the QM region described at the B3LYP DFT level. These simulations determined the free energy landscape of the process and the species along the reaction path (Figure 1B).

The findings suggested that the acylation and deacylation steps in M^{pro} proceed differently from textbook cysteine proteases (Cps) such as papain or cathepsins. Specifically, the reaction starts from a neutral His41/Cys145 catalytic dyad, while for the other enzymes, the catalytic dyad is believed to exist in the $CysS^{-}/HisH^{+}$ ion pair form in the Michaelis complex. Then, the imidazole of His41 activates the thiol of Cys145 for the nucleophilic attack on the carbonyl carbon atom of the peptide bond. The subsequent cleavage of the peptide bond is assisted by proton transfer from the protonated His41 to the nitrogen atom of the substrate, forming an acyl−enzyme complex intermediate (E-I2 in Figure 1).

While the acylation mechanism was found to be similar in both studies,[13,15] and the reaction energy barriers found in both studies were consistent with experimental values, differences arose in the deacylation step. For the fluorescently tagged polypeptide, the catalytic His deprotonated a water molecule involved in hydrolyzing the acyl-enzyme. In contrast, for the nsp4 and nsp5 peptide, the water molecule was deprotonated by the amino leaving group of the substrate. The difference in mechanism probably stems from the different leaving groups: in the former, the leaving group is "anilinic", with the electron pair of the nitrogen in direct resonance with the coumarin scaffold of the ACC fluorescent group. In the nsp4/nsp5 peptide, however, the amino leaving group is highly basic, making it more reactive. These findings highlight how subtle changes in reactant properties can influence the reaction mechanism and demonstrate the adaptability of the enzyme.

Theses mechanistic studies, combined with experimental structural biology studies, provided a foundation for simulating the inhibition of M^{pro}. The most effective inhibitors used so far are covalent agents in which an electrophilic cysteine reactive group is installed on a peptidomimetic scaffold, exemplified by the nitrile drug nirmatrelvir (the active ingredient in Paxlovid) developed by Pfizer.[17] M^{pro} inhibitors often feature a peptidomimetic scaffold that includes a glutamine residue, or a bioisostere, at the P1 position to give potency and selectivity, and branched hydrophobic substituents at both P2 and P3 positions.[11] QM/MM simulations have shed light on the mechanisms by which various electrophilic warheads inhibit M^{pro}. Warheads such as Michael acceptors,[18,19] activated carbonyl derivatives (e.g., alpha-ketoamides[20] and aldehydes[21]), hydroxymethylketones,[22,23] and nitriles[24,25] form covalent bonds with the nucleophilic Cys145 (see Figure 2).

These compounds can be categorized by the type of reactive group, or "warhead", they contain (Figure 2). Michael acceptors form a thioether through an alkylation reaction. Compounds with an activated carbonyl derivative, such as alpha-ketoamides,

https://doi.org/10.1021/acs.jpclett.4c03654
J. Phys. Chem. Lett. 2025, 16, 3249−3263

aldehydes, or hydroxymethylketones, form a thiohemiketal product. Inhibitors with a nitrile warhead undergo a Pinner reaction, forming a thioimidate product.

The inhibition mechanism of Michael acceptors involves the formation of a thioether adduct with catalytic cysteine. In contrast, activated carbonyls, acylating/carbamoylating agents, and nitriles inhibit CPs through a mechanism resembling that of the natural substrate in the acylation step of the proteolysis reaction. This mechanism generates either tetrahedral intermediate (TI) analogues (for activated carbonyl derivatives, Figure 3) or acylenzyme analogues (for nitrile derivatives and acylating/carbamoylating agents). The reversibility and irreversibility of inhibition depend on the stability of these covalent complexes, which is influenced by the nature of the warhead.

QM/MM simulations of the N3 peptidyl Michael acceptor indicate that inhibition occurs first by the formation of the $CysS^{-}/HisH^{+}$ ion pair, followed by the formation of a covalent bond between the enzyme and the inhibitor. This second step has been proposed to occur by direct reaction between the enzyme and the inhibitor[18] or through a proton shuttle involving a water molecule.[19] Both studies agree that Michael addition is the rate-determining step. However, while both define the reactant complex in its neutral dyad (E:I) as the most stable state, Arafet et al.[18] reports the formation of the ion pair to be more favorable (1.3 kcal/mol) compared to the result of Ramos-Guzman et al.[19] (10.7 kcal/mol). This difference probably accounts for the variation in the computed activation free energies (11.2 vs 21.3 kcal/mol). The low activation free energy is consistent with a diffusion-limited reaction scenario reported against SARS-CoV-2 (between 11 and 12 kcal/mol)[27] where the rate for covalent bond formation, k_3, is too fast to be measured.[11] However, high energy activation barriers are consistent with studies for which an experimental rate constant of 3.1×10^{-3} s^{-1} was reported against previous SARS-CoV M^{pro} (or 21.2 accordingly to the transition state theory).[28]

Additionally, with regard to the differences in the experimental setups, the observed differences in reaction mechanisms and free energy barriers between different QM/MM studies can be attributed to variations in QM treatment levels and sampling methods. Arafet et al.[18] studied the system at the AM1/MM level, with M06-2X corrections and Ramos-Guzman et al.[19] at the B3LYP/MM level. This is a good example about how different QM methods (e.g., different density functionals) can give very different barriers for reaction, and this is typically the most important factor in differences between QM/MM barriers for the same mechanism calculated at different levels of theory[29] and different QM region sizes.[30] Chemically accurate barriers (i.e., within 1 kcal/mol of experiment) can only be guaranteed with computationally expensive correlated ab initio QM methods, but lower level QM/MM calculations can give qualitatively useful results (and reaction energetics close to high level calculations, and to experiments, in some cases as here for M^{pro}, with an appropriate choice e.g. of density functional), identify mechanisms, and, e.g., predict relative reactivity across a series of substrates. Differences in reaction barriers can also be caused by differences in protein and/or substrate conformation;[31] reaction will proceed via such reactive conformations, but these may differ even subtly from stable structures derived from crystallography.

A similar proton shuttle mechanism was found in B3LYP/MM simulations of inhibitors containing aldehyde[21] or nitrile[25] warheads, with the proton from His41 transferred via a water molecule, rather than directly to the inhibitor; the water molecule mirrors the role of the amino leaving group in the natural substrate. The barriers obtained for these mechanisms (18.5 and 16.3 kcal/mol, respectively) were consistent with experimental kinetic data when available (2.45×10^{-3} s^{-1} for the structurally similar GC373 aldehyde,[32] value not measured for nirmatrelvir). When a hydroxyl group is included in the structure of the inhibitor, a similar indirect proton transfer reaction mechanism is observed.[21,22] The hydroxyl group mediates proton transfer from His41 to the oxygen atom of the carbonyl group, facilitating the nucleophilic attack that eventually forms a stable thiohemiketal intermediate[21,22] (Figure 3). For this reaction, the barriers reported are 15.2 kcal/mol at the AM1/MM level, with M06-2X corrections for the B4 proposed compound and 19.7 kcal/mol at the B3LYP/MM level for the PF-00835231 inhibitor. The catalytic constant (k_3) for the inhibition of the enzyme has not been experimentally measured or explicitly reported in the literature for none of them.

A similar two-step mechanisms was found at the AM1/MM level with M06-2X corrections for the reaction with a proposed, B3,[22] peptidyl covalent inhibitor, which share the same recognition motif but feature distinct cysteine-targeting warhead: a methyl oxo-enoate (a type of activated carbonyl). The rate-limiting step corresponds to the nucleophilic attack of the Cy145 sulfur atom on the inhibitor, with an activation free energy of 13.5 kcal/mol (no experimental validation available).[22] However, some mechanistic differences were noted. In the case of the methyl oxo-enoate, the nucleophilic attack on the Cα of the double bond of the Michael acceptor occurs concertedly with the direct proton transfer from His41 to Cβ. In contrast, for the hydroxymethyl ketone inhibitor mentioned in the previous paragraph, the proton transfer from H41 to the carbonyl oxygen takes place via the hydroxyl group of the inhibitor.[22]

In inhibitor design, it is generally important to focus on compounds with favorable (exergonic) covalent product (E-I) formation, and usually with low activation energy barriers to ensure kinetic feasibility (although not too reactive, to avoid off-target binding[33]). The energy barrier separating the E-I complex and the noncovalent state (E:I) determines whether an inhibitor acts irreversibly or with a reversible mechanism of action. The structure of a covalent inhibitor can be tuned to balance the benefits of irreversible inhibitors, such as enhanced in vivo potency, with those of a reversible inhibitors, which display a better toxicity profile.[34] QM/MM simulations provide a good tool to investigate these reactivity properties of covalent inhibitors within their protein targets.[35,36]

In addition to covalent inhibitors, considerable efforts have been directed toward identifying noncovalent inhibitors of M^{pro}. One prominent example is the COVID Moonshot initiative mentioned above, which led to the discovery of numerous novel hits active in biochemical and live virus assays.[3] This project leveraged the expertise of molecular designers worldwide through crowdsourcing, while simulations, including free energy perturbation (FEP), guided the hit-to-lead and lead optimization stages. This enabled the rapid identification and refinement of potential inhibitors.

Other efforts also applied molecular simulations to identify noncovalent inhibitors of SARS-CoV-2 M^{pro}. A virtual screening campaign of approved drugs performed by Jorgensen and colleagues identified significant hits,[37,38] which were then wisely exploited by the same group of investigators to discover new potent drug-like inhibitors of M^{pro}. For instance, the antiepileptic medication perampanel was the target of an

https://doi.org/10.1021/acs.jpclett.4c03654
J. Phys. Chem. Lett. 2025, 16, 3249−3263

efficient optimization process on the basis of docking and free-energy simulations. FEP results prompted the selection of 3-pyridinyl and 3-chlrophenyl groups for the S1 and S2 pockets and repositioning of the pyridinone carbonyl group. These ideas were embodied in modeling, synthesis, and testing of new compounds acting in the low micromolar range. Follow-up optimization led to several new M^{pro} inhibitors with nanomolar potency.[39] In another study,[38] compounds with a pyridinone core and substituted five-membered-ring heterocycles binding in the S4 pocket of M^{pro} and an *N*-methylated uracil ring were subjected to FEP simulations to guide the choice of heterocycles. Crystallography confirmed the desired S4 placement, and kinetics showed EC_{50} values as low as 0.080 μM (compare remdesivir at 0.5−2 μM), and IC_{50} values as low as 0.044 μM.[38] These studies demonstrate the power of computational medicinal chemistry for lead discovery, especially FEP-guided lead optimization.

Other molecular simulation techniques have also facilitated the interactive exploration of M^{pro} binding interactions. Interactive molecular dynamics in virtual reality (iMD-VR) enabled researchers in different locations to collaboratively build and analyze complexes of M^{pro} with inhibitors and substrates.[40] This iMD-VR approach was used to model complexes of designed peptide inhibitors with M^{pro}, which were experimentally validated as competitive inhibitors. A range of biomolecular simulation techniques, including automated docking, MD and iMD-VR, QM/MM, and linear-scale DFT, was used to investigate binding of 11 M^{pro} substrates (derived from viral polyprotein) and designed peptide inhibitors. The resulting binding modes were compared with previous crystallographic findings for inhibitors.[41]

In a general note of caution, we emphasize that docking methods have limited scope and accuracy (and show false positives and negatives) for noncovalent and covalent ligands for M^{pro}, necessitating complementary techniques (e.g., molecular simulation such as MD, Monte Carlo, or FEP methods).[42] Simulations of M^{pro} using Gaussian accelerated MD showed variable plasticity and novel cryptic pockets adjacent to the S2 site and other areas, such as a potentially druggable allosteric site at the M^{pro} dimer interface.[43] A follow-on study, using the AMOEBA polarizable force field, further explored the structural dynamics of M^{pro} under different pH conditions.[44] This study revealed additional cryptic pockets (which could be targets for drug design) not seen with conventional fixed-charge force fields and also showed how a change in protonation states structurally disrupted the oxyanion hole.

Resistance to M^{pro} inhibitors can arise, e.g., in response to drug treatment. A combination of theory, computation, and experiments (evolution- and structure-guided approaches)[45] investigated whether circulating variants of M^{pro} confer resistance to drugs such as nirmatrelvir and ensitrelvir. This emphasizes the need for the development of a second generation of M^{pro} inhibitors and other antiviral drugs. Notably, some M^{pro} variants resistant to nirmatrelvir remain fully susceptible to ensitrelvir and *vice versa* due to their distinct mechanisms of action.

The substrate-envelope hypothesis was used to design inhibitors that may be less likely to face resistance. The aim of this approach is that any mutation weakening inhibitor binding would also disrupt natural substrate binding. Potent, ligand-efficient, and geometrically compact inhibitors that fit tightly within the active site substrate pocket were developed. A campaign using experimental methods such as crystallographic fragment screen, synthesis, assays, in vitro and in vivo experiments, and computational tools based on machine learning, artificial intelligence (AI) and biomolecular simulations, led to the discovery of a potent noncovalent, nonpeptidic inhibitor (MAT-POS-e194df51-1) with confirmed cross reactivity against Alpha, Beta, Delta, and Omicron variants.[3] This lead-like compound has potent cellular activity without measurable cytotoxicity and (as shown by crystallography) with a different pattern of interactions with the M^{pro} binding site from nirmatrelvir and ensitrelvir, suggesting potential for complementary resistance profiles and further development.

Dynamical-nonequilibrium molecular dynamics (D-NEMD) simulations of M^{pro} identified sites known to be associated with drug resistance and allosteric binding.[46,47] These D-NEMD simulations evaluated the structural and dynamical responses of the enzyme to substrate removal: they revealed communication networks between subunits, indicating cooperativity between the subunits, and linking the active site with a known allosteric binding site.[48] Significantly perturbed regions are associated with nirmatrelvir resistance, suggesting that some mutations cause resistance by altering the allosteric behavior of the enzyme. In other simulation work, MM/GBSA analyses showed that the E166V mutation reduces the binding affinity of nirmatrelvir, and QM/MM modeling of the reaction mechanism showed a higher activation free energy for covalent complex formation in this mutant, which contributes to resistance.[49]

Overall, simulations played a key role in accelerating inhibitor discovery. Mechanistic investigations on M^{pro} rapidly found that the Cys145/His41 catalytic pair shows remarkable reactivity,[13,15] anticipating that mild electrophiles such as nitriles (i.e., nirmatrelvir) could be effective covalent inhibitors. Other simulation strategies allowed for the discovery of new potential anti-Covid agents. In the Moonshot initiative, supervised virtual screening approaches using commercial libraries, with efficient FEP simulations, discovered new orally available clinical candidates with noncovalent mechanisms of action.[3] Notable results were obtained by Jorgensen from virtual screening of a library of well chosen FDA approved agents, and chemical intuition, followed by FEP-guided optimization which yielded potent, competitive, drug-like M^{pro} inhibitors.[38,39] Molecular simulations also contributed in exploring alternative strategies to inhibit M^{pro}, such as the search for allosteric inhibitors[48] and the design of noncleavable substrate-inspired peptide agents.[41] These last activities grew out of an international collaboration to characterize M^{pro} substrates and their binding and turnover and design and test peptide inhibitors; this brought together computational and experimental expertise from the UK, Spain, France, and Italy, which involved weekly virtual meetings in COVID lockdowns. Such virtual meetings and collaborations were a feature of the pandemic and part of the experience of many researchers in that time, and many produced important results.

THE SPIKE PROTEIN

The spike glycoprotein, whose three-dimensional shape has become familiar due to its frequent depiction in representations of the virus, is a key component of SARS-CoV-2. The spike is essential for mediating cell entry and is the primary target for immune recognition.[50−54] Since the emergence of COVID-19, the spike has undergone many changes in its sequence, resulting in distinct structural, immunological, and functional features of virus variants including Alpha, Beta, Delta, and Omicron.[55,56] High-resolution imaging techniques, cryoEM in particular, have

https://doi.org/10.1021/acs.jpclett.4c03654
J. Phys. Chem. Lett. 2025, 16, 3249−3263

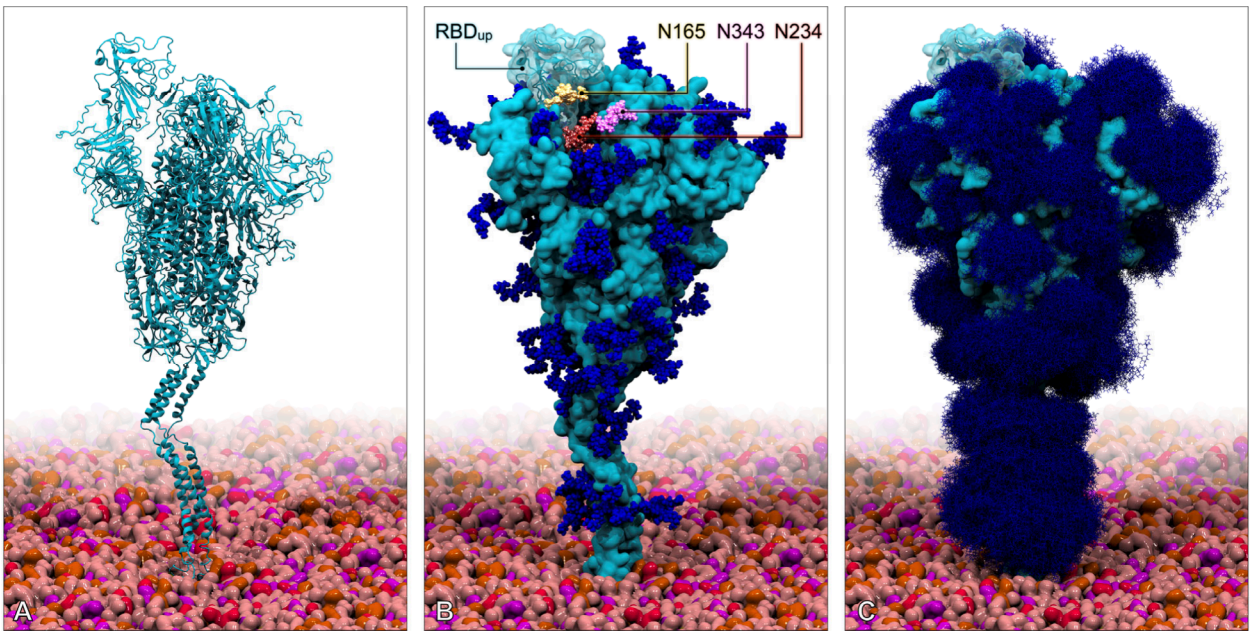

Figure 4. Full-length, fully glycosylated all-atom model of the SARS-CoV-2 spike glycoprotein. (A) The full-length, unglycosylated model of the spike protein from Casalino et al.[54] is depicted with a cartoon representation and colored in cyan, whereas the virus membrane is shown as a glossy surface, with pink, red, orange, and purple colors indicating different types of phospholipids. Cholesterol (yellow) is not visible in this representation, and glycans are not shown. Hinge points located at the membrane interface (ankle), in the middle of the spike's stalk (knee), and between the spike's stalk and the head (hip) confer remarkable flexibility. (B) The full-length, fully glycosylated model of the spike glycoprotein is represented using a cyan surface for the protein residues, whereas the N-linked glycans are depicted using blue vdW spheres. The N-glycans stabilizing the RBD in the "up" conformation, N165 and N234, or mediating the down-to-up transition, N343, are highlighted with distinct colors. (C) In this molecular representation of the full-length, fully glycosylated model of the spike glycoprotein, the glycan shield is depicted by overlaying multiple conformations obtained for each glycan in μs-scale MD simulation,[54] giving the spike a "furry" look, showing how the glycans shield it from immune recognition.

characterized the detailed architecture of the protein structure,[50−53,57] but generally N-linked and O-linked glycans are only resolved up to the first two or three monosaccharides due to the high degree of conformational variability imparted by the glycosidic linkages.[58] Additionally, some expression systems also produce spikes with limited glycosylation. Computational modeling and MD simulations have played—and continue to play—a crucial role in filling these gaps and in aiding the interpretation of experimental data. By leveraging the foundational structural data provided by cryoEM and crystal structures, resolved accurately with unprecedented speed during the early stages of the COVID-19 pandemic, molecular simulations have uncovered novel, crucial insights into the spike's structure, dynamics, and interactions.

Building on cryo-EM structures of the ectodomain head region,[50,51] advanced computational modeling enabled the construction of comprehensive, fully glycosylated, full-length models of the spike glycoprotein (Figure 4A−C).[54,59,60] These highly detailed models predicted the positions and structure of all the spike residues that were missing from the cryoEM structures, including those in the topological domains that are mostly invisible to the imaging technique or not included in the experimental structure, i.e., the stalk linking to the transmembrane domain, and the cytosolic tail (Figure 4A).[54,59,60] All the N-linked and O-linked glycans were modeled in their full-length structures based on glycomics data specifying the native glycan profiles (Figure 4B).[53,61] The resulting models, also including S-palmitoylated cysteines within the cytosolic tail, were embedded in a membrane bilayer with a biologically relevant composition (Figure 4A−C).

Explicitly solvated, all-atom MD simulations showed how N- and O-linked glycans act to shield the spike protein surface from the human immune system (see Figure 4C), as well as how the shielding changes in different conformational states, e.g., receptor binding domain (RBD) "up" vs "down" (see Figure 4B,C).[54,62] Notably, analysis of the simulations indicated a novel functional role for the glycans at N165 and N234 in structurally stabilizing the RBD in the "up" conformation (see Figure 4B),[54] thus priming the spike for host-cell attachment and infection. In subsequent work, an enhanced sampling technique called weighted ensemble (WE) path sampling[63,64] enabled detailed reconstruction of spike opening pathways from the closed (RBD "down") to open (RBD "up") states.[65] Analysis of the opening pathways (together with experiments) indicated that the glycan at N343 acted as a "glycan gate" mediating the RBD transition into the open conformation (see Figure 4B).[65] Hence, molecular simulations were key in illuminating the vulnerabilities of the glycan shield[54,62] as well as in establishing a new functional role for N-linked glycans in biological systems.[54,65,66] These works both expanded concepts of fundamental glycobiology and demonstrated how molecular simulations can serve as a basis for transformative discovery. For instance, Shapiro and colleagues[67] leveraged these simulations in their research, reporting cryoEM and crystal structures of seven potent NTD-directed neutralizing antibodies in complex with the spike protein or isolated NTD. Similarly, Guesaman et al.[68] exploited the computational findings described above to elucidate the binding mode of an antiviral lectin to spike glycans, leading to the cross-linking of spikes into soluble aggregates and potent inhibition of viral entry.

https://doi.org/10.1021/acs.jpclett.4c03654
J. Phys. Chem. Lett. 2025, 16, 3249−3263

In addition to investigating the role of the spike's N- and O-linked glycans, MD simulations have also elucidated the complex interactions between the spike protein and glycosaminoglycans (GAGs) on the host cell surface.[69−71] In all cases, hand-in-hand with experiments, simulations played an integral role in the discovery process, showcasing the power of integrated efforts for enriching our understanding of glycobiology. More recently, μs-scale MD simulations (powered by high-performance cloud-computing and unsupervised density-driven adaptive sampling) of the fully glycosylated spike in the open and closed states investigated the role of solvent.[72] These simulations suggested that water molecules provide structural support to the spike's "up" state by facilitating the formation of an interaction network involving glycans at N165/N343.

MD simulations were pivotal in revealing the vulnerabilities of the RBD, the immunodominant domain of the spike, especially during its transition from the "down" to the "up" state. Not only does the accessibility of the antigenic epitopes located on the RBD dramatically increase during opening,[54,65] but also additional sites of vulnerabilities, including druggable cryptic pockets, were found to open readily.[73,74] One of them is a pocket in proximity to the hinge region at the base of the RBD that was found to exist only when the RBD is in the open state.[73] In the same work, and in subsequent efforts, a combination of simulation techniques, including standard MD, steered MD, and umbrella sampling, characterized the free energy landscapes associated with RBD opening.[73,75] Simulations also played a crucial role in the identification of another, conserved fatty acid binding pocket in the spike's RBD and in showing that binding of linoleic acid at this site locks the spike in a noninfective conformation.[76] This newly identified site is functionally relevant to the virus. Reanalysis of the MERS and SARS-CoV spikes showed that equivalent sites also exist in them. Simulations also identified ligands for this potentially druggable site,[77] some of which have subsequently been experimentally verified.[78] D-NEMD simulations have shown that linoleate binding at this site affects distant, functionally important regions of the spike protein, and that these responses differ between variants.[79−82] They also showed that the fatty acid binding site is connected to another recently identified allosteric binding site, which binds heme and biliverdin.[83]

MD simulations have also proven useful to explore other spike regions. For example, the furin cleavage site (FCS) has attracted great interest: this region is cleaved in the process of spike "priming", and exhibits considerable flexibility and glycan shielding.[84] MD simulations were used to test the suggestion of Changeux et al.[85] that a region of the spike adjacent to the FCS may bind to nicotinic acetylcholine receptors.[84] These simulations indicated, with recent experimental support,[86] that a peptide from this FCS region has significant affinity and that this region is accessible for binding in the S1−S2 cleaved, fully glycosylated spike.[84] They also indicate differences in response between receptor subtypes. In another computational study supported by experiments, it was shown that the SARS-CoV-2 spike's FCS exhibits sequence and structural properties similar to those of the bacterial superantigen staphylococcal enterotoxin B (SEB). It was shown that the FCS can interact with T cell receptor (TCR) Vβ CDRs in a similar fashion as SEB with TCRVβ.[87]

Another area of intense research revolves around the characterization of the spike-ACE2 interaction complex. MD simulations of the fully glycosylated, full-length, membrane-bound human ACE2 receptor with the spike's RBD provided insights into the role of ACE2 in viral infection.[88,89] These studies revealed the ACE2 N-glycans involved in stabilizing RBD binding, and the inherent flexibility of the ACE2 dimer, facilitating cross-binding to multiple spikes.[88] Further molecular simulations of the RBD-ACE2 complex,[90−92] of the spike ectodomain-ACE2,[93] and of the full-length spike-ACE2[94] pinpointed the molecular determinants of this "handshake" leading to infection, shedding light on the role of glycans during target recognition and on allosteric communication between ACE2 and the spike. The spike, the RBD in particular, is subject to intense selective pressure to escape immune response,[56] and simulations have been useful in giving early views of new variants of concern, revealing how mutations in the spike protein affect its structural dynamics, binding to ACE2, or antigenic properties.[95−100]

Molecular modeling and simulations have also been demonstrated to be useful in the context of vaccine design: indirectly, by illuminating the vulnerabilities and the accessibility of the immunogenic domains in different conformational states,[54,62,101] or more directly when used as a basis to predict new epitopes[102] and to test the stability and structure of designed proteins as vaccine candidates.[103] Of particular interest for vaccine development purposes is the spike's S2 subunit. Due to its immunogenic properties and sequence conservation across different coronaviruses and SARS-CoV-2 variants of concern, the S2 subunit is deemed an ideal basis for a pan-coronavirus vaccine. Dodero-Rojas et al.[104] performed thousands of simulations based on a structure-based (Gō-like) all-atom model with simplified energetics[105,106] to investigate the transition of the S2 subunit between the prefusion and postfusion conformations, providing insights into intermediate conformations that could be used for vaccine design. In a more recent study by Nuqui et al.[107] a computational approach incorporating conventional MD simulations, WE simulations, and alchemical nonequilibrium free energy calculations was adopted to design stable SARS-CoV-S2 immunogens. In this work, cavity-filling tryptophan substitutions were introduced in the central helices, stabilizing S2 in the closed prefusion conformation. The strategic tryptophan substitutions were shown to increase the expression yield of the engineered S2 construct named "HexaPro-SS-2W", which was then also structurally resolved in the closed prefusion conformation by means of cryoEM. Immunogenic assays demonstrated its ability to elicit neutralizing responses against different SARS-CoV-2 variants, holding promise for next-generation coronavirus vaccines.[107]

MD simulations have also provided insights into how the spike protein behaves in different environments, such as on the crowded surface of the viral particle and inside a respiratory aerosol. Simulations of a patch of the viral surface, drawn from integrating cryoEM with cryo-electron tomography data, elucidated how the spike protein interacts with neighboring spike proteins on the virion.[60] This work identified three hinge points in the spike protein (Figure 4A), dubbed the hip, knee, and ankle, which could also be detected in the static cryoET structural data. Importantly, simulations of the crowded viral patch showed plasticity of the spike protein, which was not evident in the single protein simulations. The flexibility of the spike's hinge points was also observed and characterized in AI-driven, all-atom MD simulations of an 8.5 M atom, two-parallel-membrane model of the full-length spike in complex with the full-length ACE2 dimer.[94] Subsequent MD simulations of another full-length spike model showed that glycans may play a

https://doi.org/10.1021/acs.jpclett.4c03654
J. Phys. Chem. Lett. 2025, 16, 3249−3263

role in enhancing the dynamical range of motion of the stalk's segments comprised between the hinge points.[108]

More recently, very large scale, all-atom MD simulation of the Delta variant virion in the complex environment of a submicron respiratory aerosol (~250 nm in diameter) provided the first-ever views of any virus inside a respiratory aerosol particle.[109] This colossal 1 billion atom simulation showed how the spike protein interacts with the repertoire of molecules inside respiratory aerosol particles, such as mucins, monovalent and divalent ions, albumin, and lipids. The approach to investigating the virus-containing aerosol was multiscale in nature: a composite workflow that integrated four different simulation modalities, including conventional and weighted ensemble MD simulations history-augmented Markov state models, and D-NEMD, with two AI-based methods, DeepDriveMD,[110] integrated with the WE simulations to increase sampling efficiency, and OrbNet[111] for QM calculations to assess limitations of the invariant point charge force field for how the spike interacts with calcium ions. D-NEMD simulations investigated the effects of pH changes on the spike, showing that pH changes affect functionally important regions. This large-scale collaborative project also demonstrated how complex heterogeneous composite workflows, combining cloud computing and supercomputing platforms (including exascale machines at the US National Laboratories and NSF supercomputers), can provide rapid responses to pandemic threats. A summary of the computational molecular modeling and simulation approaches employed to study M^{pro} and spike is presented in Table 1.

Table 1. Summary of Molecular Simulation Methods Applied to Investigate SARS-CoV-2 M^{pro} and Spike Proteins[a]

System	Simulation method	References
M^{pro}	Hybrid methods (QM/MM, EVB)	13, 15, 18−23, 25, 36, 41, 49
	Gaussian accelerated MD	43
	Conventional MD	25, 37, 41, 45, 49
	AMOEBA MD	44
	Free energy perturbation	38, 39
	Alchemical free energy calculations	24, 25
	iMD-VR	40, 41
	D-NEMD	46
Spike	Conventional MD	54, 59, 60, 62, 66, 69−71, 76, 77, 84, 87−91, 93−101, 108, 109
	Weighted ensemble MD	65, 107, 109
	AMOEBA MD	72
	Steered MD	73
	Umbrella sampling	73, 75
	gREST MD	74
	D-NEMD	79−81
	Elastic network models	91
	Lattice models	92
	Mesoscale MD	94, 109
	Brownian dynamics	70
	DFT calculations	96
	OrbNet calculations	109
	Gō-like models	104−106
	Alchemical free energy calculations	107

[a]The table lists various molecular simulation approaches with some corresponding representative references highlighting their application; this is not a list of all such studies.

CONCLUSIONS AND OUTLOOK

SARS-CoV-2 presented the biomolecular simulation community with a situation that tested models, methods, and ways of working and sharing of data. The COVID pandemic impacted what work was done, how it was done, and the pace at which such work was accomplished. Simulations provided valuable insight into the molecular details of the virus and its lifecycle, beyond that available from experiment, and contributed to practical developments of inhibitors and vaccines. Work in the pandemic also revealed challenges and areas for improvement. The main strengths and challenges discussed in this review are summarized below.

Some Strengths.

- Simulations proved useful in revealing molecular details of structures, interactions, dynamics, and mechanisms, allowing scientists to integrate data from many types of experiments to make informative, predictive models relatively quickly.
- The simulation community showed how we could quickly unify to address this threat collaboratively: (i) the community of compute providers established a framework for quick delivery of compute cycles for SARS-CoV-2 applications and (ii) the simulation community developed new, large-scale efforts for sharing of models, methods, and data.[5] This helped make methods and findings more robust and reproducible and increased reuse and trustability of simulation results. Active collaboration with experimental researchers led to rapid exploitation of results, exchange of knowledge, and refinement of models and greatly accelerated progress. The simulation community should continue to develop in these directions, across projects, areas, and investigators.[112] These efforts take on even more importance with the rise of machine learning and the promise of AI to transform biological research.
- Simulations illuminated mechanisms outside the direct reach of experiment, including the catalytic mechanism of M^{pro}, with substrates and inhibitors as well as spike structure (e.g., glycosylation) and infection mechanisms.
- Simulations provided a basis for foundational discoveries, such as discovering a new role for N-glycans in biology (literally rewriting the glycobiology textbooks).
- Simulations played a key role in identifying and developing M^{pro} inhibitors and identifying ligands of the spike protein.
- Composite multiscale AI-driven workflows show how different types of simulation methods, run on a diversity of computer architectures, can be practically combined to address a question; such techniques will be increasingly important, including for future pandemic threats.

Some Challenges.

- Communicating findings to the broader scientific community and to the public: to have impact, the simulation community has to engage with the broader scientific community, particularly experimentalists working on similar questions. Examples from the pandemic showed the increased impact of work integrating simulations with experiments, with simulations contributing to experimental design and interpretation, and accelerating discovery and development. Even more

https://doi.org/10.1021/acs.jpclett.4c03654
J. Phys. Chem. Lett. 2025, 16, 3249−3263

challenging is the need to effectively convey complex scientific findings to a nonspecialist audience. This includes translating technical jargon into accessible language and images without oversimplifying the science, ensuring the public understands the relevance and implications of our research.

- Data sharing/analysis/transfer: As the volume and complexity of data continue to grow, managing, sharing, and analyzing these data become increasingly difficult.[112] Advanced computational resources and infrastructure are required to handle big data, posing logistical and financial sustainability challenges. The US National Data Platform is a potential appealing solution that has been designed with AI-readiness in mind.[113] Another notable initiative is the Molecular Dynamics Database (https://mddbr.eu).[5,114] Effective data storage, allowing analysis and reuse of simulation data will allow training of machine learning models and facilitate AI-driven simulations.
- Docking methods showed mixed results, generating many false positives and false negatives, and generally lacking predictive value for binding affinities;[42] on the other hand, docking, while simple, was an essential starting point for several successful efforts in ligand and inhibitor discovery and development.
- Data visualization, which is crucial for understanding and instrumental for discovery, becomes increasingly challenging as the size and complexity of systems increase. Traditional visualization tools and techniques for biomolecular dynamics can struggle with large-scale data, necessitating the development of new methods to interpret and present data effectively. Interactive virtual reality offers promise here, and in facilitating virtual collaboration.
- Building realistic models of some targets is challenging, for example including post-translational modifications such as glycosylation of the spike, and unexpected ligands. Simulations have shown the critical role of glycans in the spike, in immune shielded and also in modulating its dynamics. While simulations of the unglycosylated spike have been useful for some purposes (e.g., in identifying allosteric effects), they cannot describe its interactions. Modeling glycosylation accurately is challenging, and glycosylation may vary across and within variants. Uncertainties in structural models should be considered, and the significance of results should be tested.
- Ensuring reproducibility of results across different laboratories and studies is critical for scientific progress. Standardizing modeling approaches, simulation protocols, and data formats can help, and publication and sharing of these details is essential, but achieving this across diverse research environments internationally remains complex.

AUTHOR INFORMATION

Corresponding Authors

Rommie E. Amaro − *Department of Molecular Biology, University of California San Diego, La Jolla, California 92093, United States;* orcid.org/0000-0002-9275-9553; Email: ramaro@ucsd.edu

Carlos Simmerling − *Department of Chemistry and Laufer Center for Physical and Quantitative Biology, Stony Brook University, Stony Brook, New York 11794-3400, United States;* orcid.org/0000-0002-7252-4730; Email: carlos.simmerling@stonybrook.edu

Alessio Lodola − *Dipartimento di Scienze degli Alimenti e del Farmaco, Università degli Studi di Parma, I 43121 Parma, Italy;* orcid.org/0000-0002-8675-1002; Email: alessio.lodola@unipr.it

Adrian J. Mulholland − *Centre for Computational Chemistry, School of Chemistry, University of Bristol, Bristol BS8 1TS, United Kingdom;* orcid.org/0000-0003-1015-4567; Email: adrian.mulholland@bristol.ac.uk

Katarzyna Świderek − *Biocomp group, Institute of Advanced Materials (INAM), Universitat Jaume I, 12071 Castelló, Spain;* orcid.org/0000-0002-7528-1551; Email: swiderek@uji.es

Vicent Moliner − *Biocomp group, Institute of Advanced Materials (INAM), Universitat Jaume I, 12071 Castelló, Spain;* orcid.org/0000-0002-3665-3391; Email: moliner@uji.es

Authors

Lorenzo Casalino − *Department of Molecular Biology, University of California San Diego, La Jolla, California 92093, United States;* orcid.org/0000-0003-3581-1148

Carlos A. Ramos-Guzmán − *Centre for Computational Chemistry, School of Chemistry, University of Bristol, Bristol BS8 1TS, United Kingdom;* orcid.org/0000-0002-7701-377X

Complete contact information is available at: https://pubs.acs.org/10.1021/acs.jpclett.4c03654

Notes

The authors declare no competing financial interest.

Biographies

Lorenzo Casalino earned his M.Sc. in Pharmaceutical Chemistry and Technology from the University of Milan, Italy, in 2013. In 2017, he received his Ph.D. in Computational Biophysics from the International School for Advanced Studies (SISSA), Trieste, Italy. In 2018, he joined Prof. Rommie Amaro's lab at the University of California, San Diego, as a postdoctoral scholar and has held the position of assistant project scientist since 2023. His research focuses on multiscale modeling and simulations of viruses, including SARS-CoV-2, influenza, and HIV-1 viruses. In recognition of his contributions to COVID-19 research, Lorenzo was awarded the 2020 ACM Gordon Bell Special Prize for COVID-19 research.

Carlos A. Ramos-Guzmán is a research associate in the Mulholland Research Group at the University of Bristol. Carlos received his Ph.D. in Theoretical Chemistry and Computational Modelling from the University of Valencia. His research focus is on using classical and hybrid quantum mechanical/molecular mechanics simulation techniques to combat infectious diseases caused by viruses like SARS-CoV-2 and antimicrobial-resistant bacteria.

Rommie E. Amaro holds the Distinguished Professorship in Theoretical and Computational Chemistry at the University of California, San Diego. She received her B.S. in Chemical Engineering (1999) and her Ph.D. in Chemistry (2005) from the University of Illinois at Urbana−Champaign. She is the recipient of an NIH New Innovator Award, the Presidential Early Career Award for Scientists and Engineers, the ACS Kavli Foundation Emerging Leader in Chemistry, the Corwin Hansch Award, and the 2020 ACM Gordon Bell Special Prize for COVID19. Rommie's scientific vision revolves around expanding the range and complexity of molecular constituents represented in atomic-level molecular dynamics simulations and the

https://doi.org/10.1021/acs.jpclett.4c03654
J. Phys. Chem. Lett. 2025, 16, 3249−3263

development of novel multiscale methods for elucidating their time dependent dynamics.

Carlos Simmerling is the Marsha Laufer Chair of Physical & Quantitative Biology at Stony Brook University and a Fellow of the American Chemical Society. His research focuses on development of improved molecular simulation methods and energy functions, and he is a lead developer of the Amber biomolecular simulation software that is used in thousands of research laboratories worldwide. He also uses these tools to study biomolecular recognition mechanisms, working closely with collaborators to help guide and interpret their experiments.

Alessio Lodola received his Ph.D. in Medicinal Chemistry from the University of Pavia. After a stint as visiting researcher in the group of Prof. Adrian Mulholland at the University of Bristol, UK, Dr. Lodola returned to Italy where he is now Professor in Medicinal Chemistry at the University of Parma. A member of the Drug Design and Discovery group led by Prof. Mor, Dr. Lodola's research mainly centers on the use of atomistic simulations for the design of inhibitors of enzymes of pharmaceutical interest.

Adrian Mulholland is a Professor of Chemistry and a founding member of the Centre for Computational Chemistry at the University of Bristol. His research focuses on biomolecular simulation, including of enzyme catalytic mechanisms and multiscale methods. He established the collaborative computational consortia CCPBioSim (ccpbiosim.ac.uk) and HECBioSim (hecbiosim.ac.uk) and chaired the Molecular Graphics and Modelling Society (mgms.org). He is an ERC Advanced Grant holder, was the inaugural Lakshmi Raman Lecturer, University of Pittsburgh (2019), and received the 2020 JMT Medal.

Katarzyna Świderek earned her Ph.D. in Physical Chemistry from Lodz University of Technology, Poland. She has held research positions across Europe. As a principal investigator, she has led projects funded by the Spanish and Polish Ministries of Science. As a Ramón y Cajal fellow and assistant professor at Universitat Jaume I, she collaborates with international researchers on projects with pharmacological, medical, and industrial applications. Her research focuses on theoretical studies of reactivity in cellular processes, with an emphasis on biocatalysis, inhibition, and drug design, using molecular dynamics simulations with hybrid QM/MM potentials.

Vicent Moliner is Professor of Physical Chemistry at University Jaume I, where he received his Ph.D. in Chemistry (1993). He he has been visiting professor at several universities, such as the University of Bath (United Kingdom) thanks to a prize awarded by the same university (David Parkin Visiting Professor), or the Lodz University of Technology (Poland). The interest of Dr. Moliner focuses on the development of QM/MM MD methods for the study of the foundations of enzymatic reactions and applications such as the design of biocatalysts or enzymatic inhibitors.

■ ACKNOWLEDGMENTS

K.Ś. and V.M. acknowledge financial support from grant PID2021-123332OB-C21 funded by MCIN/AEI/10.13039/501100011033/and by "ERDF A way of making Europe", and from grant PROMETEO CIPROM/2021/079 of Generalitat Valenciana. K.Ś. thanks the Spanish Ministerio de Ciencia, Innovación y Universidades (Grant PID2019-107098RJ-I00). A.J.M. thanks EPSRC for support (CCP-BioSim, grant number EP/M022609/1) and also the British Society for Antimicrobial Chemotherapy (grant number BSAC-COVID-30). A.J.M. and C.A.R.-G. thank ERC for support: some of the work reported here is part of a project that has received funding from the European Research Council under the European Horizon 2020 research and innovation programme (PREDACTED Advanced Grant Agreement no. 101021207).

■ REFERENCES

(1) Mulholland, A. J.; Amaro, R. E. COVID19 - Computational Chemists Meet the Moment. *J. Chem. Inf. Model.* **2020**, *60* (12), 5724−5726.

(2) Amaro, R. E.; Mulholland, A. J. A Community Letter Regarding Sharing Biomolecular Simulation Data for COVID-19. *J. Chem. Inf. Model.* **2020**, *60* (6), 2653−2656.

(3) Boby, M. L.; Fearon, D.; Ferla, M.; Filep, M.; Koekemoer, L.; Robinson, M. C.; The COVID Moonshot Consortium‡; Chodera, J. D.; Lee, A. A.; London, N.; Von Delft, A.; Von Delft, F.; Achdout, H.; Aimon, A.; Alonzi, D. S.; Arbon, R.; Aschenbrenner, J. C.; Balcomb, B. H.; Bar-David, E.; Barr, H.; Ben-Shmuel, A.; Bennett, J.; Bilenko, V. A.; Borden, B.; Boulet, P.; Bowman, G. R.; Brewitz, L.; Brun, J.; Bvnbs, S.; Calmiano, M.; Carbery, A.; Carney, D. W.; Cattermole, E.; Chang, E.; Chernyshenko, E.; Clyde, A.; Coffland, J. E.; Cohen, G.; Cole, J. C.; Contini, A.; Cox, L.; Croll, T. I.; Cvitkovic, M.; De Jonghe, S.; Dias, A.; Donckers, K.; Dotson, D. L.; Douangamath, A.; Duberstein, S.; Dudgeon, T.; Dunnett, L. E.; Eastman, P.; Erez, N.; Eyermann, C. J.; Fairhead, M.; Fate, G.; Fedorov, O.; Fernandes, R. S.; Ferrins, L.; Foster, R.; Foster, H.; Fraisse, L.; Gabizon, R.; García-Sastre, A.; Gawriljuk, V. O.; Gehrtz, P.; Gileadi, C.; Giroud, C.; Glass, W. G.; Glen, R. C.; Glinert, I.; Godoy, A. S.; Gorichko, M.; Gorrie-Stone, T.; Griffen, E. J.; Haneef, A.; Hassell Hart, S.; Heer, J.; Henry, M.; Hill, M.; Horrell, S.; Huang, Q. Y. J.; Huliak, V. D.; Hurley, M. F. D.; Israely, T.; Jajack, A.; Jansen, J.; Jnoff, E.; Jochmans, D.; John, T.; Kaminow, B.; Kang, L.; Kantsadi, A. L.; Kenny, P. W.; Kiappes, J. L.; Kinakh, S. O.; Kovar, B.; Krojer, T.; La, V. N. T.; Laghnimi-Hahn, S.; Lefker, B. A.; Levy, H.; Lithgo, R. M.; Logvinenko, I. G.; Lukacik, P.; Macdonald, H. B.; MacLean, E. M.; Makower, L. L.; Malla, T. R.; Marples, P. G.; Matviiuk, T.; McCorkindale, W.; McGovern, B. L.; Melamed, S.; Melnykov, K. P.; Michurin, O.; Miesen, P.; Mikolajek, H.; Milne, B. F.; Minh, D.; Morris, A.; Morris, G. M.; Morwitzer, M. J.; Moustakas, D.; Mowbray, C. E.; Nakamura, A. M.; Neto, J. B.; Neyts, J.; Nguyen, L.; Noske, G. D.; Oleinikovas, V.; Oliva, G.; Overheul, G. J.; Owen, C. D.; Pai, R.; Pan, J.; Paran, N.; Payne, A. M.; Perry, B.; Pingle, M.; Pinjari, J.; Politi, B.; Powell, A.; Pšenák, V.; Pulido, I.; Puni, R.; Rangel, V. L.; Reddi, R. N.; Rees, P.; Reid, S. P.; Reid, L.; Resnick, E.; Ripka, E. G.; Robinson, R. P.; Rodriguez-Guerra, J.; Rosales, R.; Rufa, D. A.; Saar, K.; Saikatendu, K. S.; Salah, E.; Schaller, D.; Scheen, J.; Schiffer, C. A.; Schofield, C. J.; Shafeev, M.; Shaikh, A.; Shaqra, A. M.; Shi, J.; Shurrush, K.; Singh, S.; Sittner, A.; Sjö, P.; Skyner, R.; Smalley, A.; Smeets, B.; Smilova, M. D.; Solmesky, L. J.; Spencer, J.; Strain-Damerell, C.; Swamy, V.; Tamir, H.; Taylor, J. C.; Tennant, R. E.; Thompson, W.; Thompson, A.; Tomásio, S.; Tomlinson, C. W. E.; Tsurupa, I. S.; Tumber, A.; Vakonakis, I.; Van Rij, R. P.; Vangeel, L.; Varghese, F. S.; Vaschetto, M.; Vitner, E. B.; Voelz, V.; Volkamer, A.; Walsh, M. A.; Ward, W.; Weatherall, C.; Weiss, S.; White, K. M.; Wild, C. F.; Witt, K. D.; Wittmann, M.; Wright, N.; Yahalom-Ronen, Y.; Yilmaz, N. K.; Zaidmann, D.; Zhang, I.; Zidane, H.; Zitzmann, N.; Zvornicanin, S. N. Open Science Discovery of Potent Noncovalent SARS-CoV-2 Main Protease Inhibitors. *Science* **2023**, *382* (6671), No. eabo7201.

(4) Schimunek, J.; Seidl, P.; Elez, K.; Hempel, T.; Le, T.; Noé, F.; Olsson, S.; Raich, L.; Winter, R.; Gokcan, H.; Gusev, F.; Gutkin, E. M.; Isayev, O.; Kurnikova, M. G.; Narangoda, C. H.; Zubatyuk, R.; Bosko, I. P.; Furs, K. V.; Karpenko, A. D.; Kornoushenko, Y. V.; Shuldau, M.; Yushkevich, A.; Benabderrahmane, M. B.; Bousquet-Melou, P.; Bureau, R.; Charton, B.; Cirou, B. C.; Gil, G.; Allen, W. J.; Sirimulla, S.; Watowich, S.; Antonopoulos, N.; Epitropakis, N.; Krasoulis, A.; Pitsikalis, V.; Theodorakis, S.; Kozlovskii, I.; Maliutin, A.; Medvedev, A.; Popov, P.; Zaretckii, M.; Eghbal-Zadeh, H.; Halmich, C.; Hochreiter, S.; Mayr, A.; Ruch, P.; Widrich, M.; Berenger, F.; Kumar, A.; Yamanishi, Y.; Zhang, K. Y. J.; Bengio, E.; Bengio, Y.; Jain, M. J.; Korablyov, M.; Liu, C.; Marcou, G.; Glaab, E.; Barnsley, K.; Iyengar, S. M.; Ondrechen, M. J.; Haupt, V. J.; Kaiser, F.; Schroeder, M.; Pugliese, L.; Albani, S.; Athanasiou, C.; Beccari, A.; Carloni, P.; D'Arrigo, G.; Gianquinto, E.; Goßen, J.; Hanke, A.; Joseph, B. P.; Kokh, D. B.;

https://doi.org/10.1021/acs.jpclett.4c03654
J. Phys. Chem. Lett. 2025, 16, 3249−3263

Kovachka, S.; Manelfi, C.; Mukherjee, G.; Muñiz-Chicharro, A.; Musiani, F.; Nunes-Alves, A.; Paiardi, G.; Rossetti, G.; Sadiq, S. K.; Spyrakis, F.; Talarico, C.; Tsengenes, A.; Wade, R. C.; Copeland, C.; Gaiser, J.; Olson, D. R.; Roy, A.; Venkatraman, V.; Wheeler, T. J.; Arthanari, H.; Blaschitz, K.; Cespugli, M.; Durmaz, V.; Fackeldey, K.; Fischer, P. D.; Gorgulla, C.; Gruber, C.; Gruber, K.; Hetmann, M.; Kinney, J. E.; Padmanabha Das, K. M.; Pandita, S.; Singh, A.; Steinkellner, G.; Tesseyre, G.; Wagner, G.; Wang, Z.; Yust, R. J.; Druzhilovskiy, D. S.; Filimonov, D. A.; Pogodin, P. V.; Poroikov, V.; Rudik, A. V.; Stolbov, L. A.; Veselovsky, A. V.; De Rosa, M.; De Simone, G.; Gulotta, M. R.; Lombino, J.; Mekni, N.; Perricone, U.; Casini, A.; Embree, A.; Gordon, D. B.; Lei, D.; Pratt, K.; Voigt, C. A.; Chen, K.; Jacob, Y.; Krischuns, T.; Lafaye, P.; Zettor, A.; Rodríguez, M. L.; White, K. M.; Fearon, D.; Von Delft, F.; Walsh, M. A.; Horvath, D.; Brooks, C. L.; Falsafi, B.; Ford, B.; García-Sastre, A.; Yup Lee, S.; Naffakh, N.; Varnek, A.; Klambauer, G.; Hermans, T. M. A Community Effort in SARS-CoV-2 Drug Discovery. *Mol. Inform.* **2024**, *43* (1), No. e202300262.

(5) Beltrán, D.; Hospital, A.; Gelpí, J. L.; Orozco, M. A New Paradigm for Molecular Dynamics Databases: The COVID-19 Database, the Legacy of a Titanic Community Effort. *Nucleic Acids Res.* **2024**, *52* (D1), D393−D403.

(6) Amaro, R. E.; Mulholland, A. J. Biomolecular Simulations in the Time of COVID-19, and After. *Comput. Sci. Eng.* **2020**, *22* (6), 30−36.

(7) Amaro, R. E.; Mulholland, A. J. Multiscale Methods in Drug Design Bridge Chemical and Biological Complexity in the Search for Cures. *Nat. Rev. Chem.* **2018**, *2* (4), 0148.

(8) Yang, Y.; Luo, Y.-D.; Zhang, C.-B.; Xiang, Y.; Bai, X.-Y.; Zhang, D.; Fu, Z.-Y.; Hao, R.-B.; Liu, X.-L. Progress in Research on Inhibitors Targeting SARS-CoV-2 Main Protease (M ^{pro}). *ACS Omega* **2024**, *9* (32), 34196−34219.

(9) Aniana, A.; Nashed, N. T.; Ghirlando, R.; Coates, L.; Kneller, D. W.; Kovalevsky, A.; Louis, J. M. Insights into the Mechanism of SARS-CoV-2 Main Protease Autocatalytic Maturation from Model Precursors. *Commun. Biol.* **2023**, *6* (1), 1159.

(10) Zhang, L.; Lin, D.; Sun, X.; Curth, U.; Drosten, C.; Sauerhering, L.; Becker, S.; Rox, K.; Hilgenfeld, R. Crystal Structure of SARS-CoV-2 Main Protease Provides a Basis for Design of Improved α-Ketoamide Inhibitors. *Science* **2020**, *368* (March), 409−412.

(11) Jin, Z.; Du, X.; Xu, Y.; Deng, Y.; Liu, M.; Zhao, Y.; Zhang, B.; Li, X.; Zhang, L.; Peng, C.; Duan, Y.; Yu, J.; Wang, L.; Yang, K.; Liu, F.; Jiang, R.; Yang, X.; You, T.; Liu, X.; Yang, X.; Bai, F.; Liu, H.; Liu, X.; Guddat, L. W.; Xu, W.; Xiao, G.; Qin, C.; Shi, Z.; Jiang, H.; Rao, Z.; Yang, H. Structure of Mpro from SARS-CoV-2 and Discovery of Its Inhibitors. *Nature* **2020**, *582* (7811), 289−293.

(12) Kneller, D. W.; Phillips, G.; Weiss, K. L.; Pant, S.; Zhang, Q.; O'Neill, H. M.; Coates, L.; Kovalevsky, A. Unusual Zwitterionic Catalytic Site of SARS−CoV-2 Main Protease Revealed by Neutron Crystallography. *J. Biol. Chem.* **2020**, *295* (50), 17365−17373.

(13) Świderek, K.; Moliner, V. Revealing the Molecular Mechanisms of Proteolysis of SARS-CoV-2 M pro by QM/MM Computational Methods. *Chem. Sci.* **2020**, *11* (39), 10626−10630.

(14) Rut, W.; Groborz, K.; Zhang, L.; Sun, X.; Zmudzinski, M.; Pawlik, B.; Wang, X.; Jochmans, D.; Neyts, J.; Młynarski, W.; Hilgenfeld, R.; Drag, M. SARS-CoV-2 Mpro Inhibitors and Activity-Based Probes for Patient-Sample Imaging. *Nat. Chem. Biol.* **2021**, *17* (2), 222−228.

(15) Ramos-Guzmán, C. A.; Ruiz-Pernía, J. J.; Tuñón, I. Unraveling the SARS-CoV-2 Main Protease Mechanism Using Multiscale Methods. *ACS Catal.* **2020**, *10* (21), 12544−12554.

(16) Greasley, S. E.; Noell, S.; Plotnikova, O.; Ferre, R.; Liu, W.; Bolanos, B.; Fennell, K.; Nicki, J.; Craig, T.; Zhu, Y.; Stewart, A. E.; Steppan, C. M. Structural Basis for the in Vitro Efficacy of Nirmatrelvir against SARS-CoV-2 Variants. *J. Biol. Chem.* **2022**, *298* (6), No. 101972.

(17) Owen, D. R.; Allerton, C. M. N.; Anderson, A. S.; Aschenbrenner, L.; Avery, M.; Berritt, S.; Boras, B.; Cardin, R. D.; Carlo, A.; Coffman, K. J.; Dantonio, A.; Di, L.; Eng, H.; Ferre, R.; Gajiwala, K. S.; Gibson, S. A.; Greasley, S. E.; Hurst, B. L.; Kadar, E. P.; Kalgutkar, A. S.; Lee, J. C.; Lee, J.; Liu, W.; Mason, S. W.; Noell, S.; Novak, J. J.; Obach, R. S.; Ogilvie, K.; Patel, N. C.; Pettersson, M.; Rai, D. K.; Reese, M. R.; Sammons, M. F.; Sathish, J. G.; Singh, R. S. P.; Steppan, C. M.; Stewart, A. E.; Tuttle, J. B.; Updyke, L.; Verhoest, P. R.; Wei, L.; Yang, Q.; Zhu, Y. An Oral SARS-CoV-2 M ^{pro} Inhibitor Clinical Candidate for the Treatment of COVID-19. *Science* **2021**, *374* (6575), 1586−1593.

(18) Arafet, K.; Serrano-Aparicio, N.; Lodola, A.; Mulholland, A. J.; González, F. V.; Świderek, K.; Moliner, V. Mechanism of Inhibition of SARS-CoV-2 M ^{pro} by N3 Peptidyl Michael Acceptor Explained by QM/MM Simulations and Design of New Derivatives with Tunable Chemical Reactivity. *Chem. Sci.* **2021**, *12* (4), 1433−1444.

(19) Ramos-Guzmán, C. A.; Ruiz-Pernía, J. J.; Tuñón, I. A Microscopic Description of SARS-CoV-2 Main Protease Inhibition with Michael Acceptors. Strategies for Improving Inhibitor Design. *Chem. Sci.* **2021**, *12* (10), 3489−3496.

(20) Mondal, D.; Warshel, A. Exploring the Mechanism of Covalent Inhibition: Simulating the Binding Free Energy of α-Ketoamide Inhibitors of the Main Protease of SARS-CoV-2. *Biochemistry* **2020**, *59* (48), 4601−4608.

(21) Ramos-Guzmán, C. A.; Ruiz-Pernía, J. J.; Tuñón, I. Multiscale Simulations of SARS-CoV-2 3CL Protease Inhibition with Aldehyde Derivatives. Role of Protein and Inhibitor Conformational Changes in the Reaction Mechanism. *ACS Catal.* **2021**, *11* (7), 4157−4168.

(22) Martí, S.; Arafet, K.; Lodola, A.; Mulholland, A. J.; Świderek, K.; Moliner, V. Impact of Warhead Modulations on the Covalent Inhibition of SARS-CoV-2 M pro Explored by QM/MM Simulations. *ACS Catal.* **2022**, *12* (1), 698−708.

(23) Ramos-Guzmán, C. A.; Ruiz-Pernía, J. J.; Tuñón, I. Inhibition Mechanism of SARS-CoV-2 Main Protease with Ketone-Based Inhibitors Unveiled by Multiscale Simulations: Insights for Improved Designs. *Angew. Chem., Int. Ed.* **2021**, *60* (49), 25933−25941.

(24) Ramos-Guzmán, C. A.; Ruiz-Pernía, J. J.; Tuñón, I. Computational Simulations on the Binding and Reactivity of a Nitrile Inhibitor of the SARS-CoV-2 Main Protease. *Chem. Commun.* **2021**, *57* (72), 9096−9099.

(25) Schillings, J.; Ramos-Guzmán, C. A.; Ruiz-Pernía, J. J.; Tuñón, I. Pomotrelvir and Nirmatrelvir Binding and Reactivity with SARS-CoV-2 Main Protease: Implications for Resistance Mechanisms from Computations. *Angew. Chem., Int. Ed.* **2024**, *63*, No. e202409527.

(26) Schechter, I.; Berger, A. On the Size of the Active Site in Proteases. I. Papain. *Biochem. Biophys. Res. Commun.* **1967**, *27* (2), 157−162.

(27) Alberty, R. A.; Hammes, G. G. Application of the Theory of Diffusion-Controlled Reactions to Enzyme Kinetics. *J. Phys. Chem.* **1958**, *62* (2), 154−159.

(28) Yang, H.; Xie, W.; Xue, X.; Yang, K.; Ma, J.; Liang, W.; Zhao, Q.; Zhou, Z.; Pei, D.; Ziebuhr, J.; Hilgenfeld, R.; Kwok, Y. Y.; Wong, L.; Gao, G.; Chen, S.; Chen, Z.; Ma, D.; Bartlam, M.; Rao, Z. Design of Wide-Spectrum Inhibitors Targeting Coronavirus Main Proteases. *PLoS Biol.* **2005**, *3* (10), e324.

(29) Ramos-Guzmán, C. A.; Velázquez-Libera, J. L.; Ruiz-Pernía, J. J.; Tuñón, I. Testing Affordable Strategies for the Computational Study of Reactivity in Cysteine Proteases: The Case of SARS-CoV-2 3CL Protease Inhibition. *J. Chem. Theory Comput.* **2022**, *18* (6), 4005−4013.

(30) Ranaghan, K. E.; Shchepanovska, D.; Bennie, S. J.; Lawan, N.; Macrae, S. J.; Zurek, J.; Manby, F. R.; Mulholland, A. J. Projector-Based Embedding Eliminates Density Functional Dependence for QM/MM Calculations of Reactions in Enzymes and Solution. *J. Chem. Inf. Model.* **2019**, *59* (5), 2063−2078.

(31) Lodola, A.; Sirirak, J.; Fey, N.; Rivara, S.; Mor, M.; Mulholland, A. J. Structural Fluctuations in Enzyme-Catalyzed Reactions: Determinants of Reactivity in Fatty Acid Amide Hydrolase from Multivariate Statistical Analysis of Quantum Mechanics/Molecular Mechanics Paths. *J. Chem. Theory Comput.* **2010**, *6* (9), 2948−2960.

(32) Ma, C.; Sacco, M. D.; Hurst, B.; Townsend, J. A.; Hu, Y.; Szeto, T.; Zhang, X.; Tarbet, B.; Marty, M. T.; Chen, Y.; Wang, J. Boceprevir, GC-376, and Calpain Inhibitors II, XII Inhibit SARS-CoV-2 Viral Replication by Targeting the Viral Main Protease. *Cell Res.* **2020**, *30* (8), 678−692.

https://doi.org/10.1021/acs.jpclett.4c03654
J. Phys. Chem. Lett. 2025, 16, 3249−3263

(33) Voice, A.; Tresadern, G.; Van Vlijmen, H.; Mulholland, A. Limitations of Ligand-Only Approaches for Predicting the Reactivity of Covalent Inhibitors. *J. Chem. Inf. Model.* **2019**, *59* (10), 4220−4227.
(34) Ghosh, A. K.; Brindisi, M.; Shahabi, D.; Chapman, M. E.; Mesecar, A. D. Drug Development and Medicinal Chemistry Efforts toward SARS-Coronavirus and Covid-19 Therapeutics. *ChemMedChem.* **2020**, *15* (11), 907−932.
(35) Lodola, A.; Mor, M.; Sirirak, J.; Mulholland, A. J. Insights into the Mechanism and Inhibition of Fatty Acid Amide Hydrolase from Quantum Mechanics/Molecular Mechanics (QM/MM) Modelling. *Biochem. Soc. Trans.* **2009**, *37* (2), 363−367.
(36) Medrano, F. J.; De La Hoz-Rodríguez, S.; Martí, S.; Arafet, K.; Schirmeister, T.; Hammerschmidt, S. J.; Müller, C.; González-Martínez, Á.; Santillana, E.; Ziebuhr, J.; Romero, A.; Zimmer, C.; Weldert, A.; Zimmermann, R.; Lodola, A.; Świderek, K.; Moliner, V.; González, F. V. Peptidyl Nitroalkene Inhibitors of Main Protease Rationalized by Computational and Crystallographic Investigations as Antivirals against SARS-CoV-2. *Commun. Chem.* **2024**, *7* (1), 15.
(37) Ghahremanpour, M. M.; Tirado-Rives, J.; Deshmukh, M.; Ippolito, J. A.; Zhang, C.-H.; Cabeza De Vaca, I.; Liosi, M.-E.; Anderson, K. S.; Jorgensen, W. L. Identification of 14 Known Drugs as Inhibitors of the Main Protease of SARS-CoV-2. *ACS Med. Chem. Lett.* **2020**, *11* (12), 2526−2533.
(38) Zhang, C.-H.; Spasov, K. A.; Reilly, R. A.; Hollander, K.; Stone, E. A.; Ippolito, J. A.; Liosi, M.-E.; Deshmukh, M. G.; Tirado-Rives, J.; Zhang, S.; Liang, Z.; Miller, S. J.; Isaacs, F.; Lindenbach, B. D.; Anderson, K. S.; Jorgensen, W. L. Optimization of Triarylpyridinone Inhibitors of the Main Protease of SARS-CoV-2 to Low-Nanomolar Antiviral Potency. *ACS Med. Chem. Lett.* **2021**, *12* (8), 1325−1332.
(39) Zhang, C.-H.; Stone, E. A.; Deshmukh, M.; Ippolito, J. A.; Ghahremanpour, M. M.; Tirado-Rives, J.; Spasov, K. A.; Zhang, S.; Takeo, Y.; Kudalkar, S. N.; Liang, Z.; Isaacs, F.; Lindenbach, B.; Miller, S. J.; Anderson, K. S.; Jorgensen, W. L. Potent Noncovalent Inhibitors of the Main Protease of SARS-CoV-2 from Molecular Sculpting of the Drug Perampanel Guided by Free Energy Perturbation Calculations. *ACS Cent. Sci.* **2021**, *7* (3), 467−475.
(40) Deeks, H. M.; Walters, R. K.; Barnoud, J.; Glowacki, D. R.; Mulholland, A. J. Interactive Molecular Dynamics in Virtual Reality Is an Effective Tool for Flexible Substrate and Inhibitor Docking to the SARS-CoV-2 Main Protease. *J. Chem. Inf. Model.* **2020**, *60* (12), 5803−5814.
(41) Chan, H. T. H.; Moesser, M. A.; Walters, R. K.; Malla, T. R.; Twidale, R. M.; John, T.; Deeks, H. M.; Johnston-Wood, T.; Mikhailov, V.; Sessions, R. B.; Dawson, W.; Salah, E.; Lukacik, P.; Strain-Damerell, C.; Owen, C. D.; Nakajima, T.; Świderek, K.; Lodola, A.; Moliner, V.; Glowacki, D. R.; Spencer, J.; Walsh, M. A.; Schofield, C. J.; Genovese, L.; Shoemark, D. K.; Mulholland, A. J.; Duarte, F.; Morris, G. M. Discovery of SARS-CoV-2 M ^{pro} Peptide Inhibitors from Modelling Substrate and Ligand Binding. *Chem. Sci.* **2021**, *12* (41), 13686−13703.
(42) Zev, S.; Raz, K.; Schwartz, R.; Tarabeh, R.; Gupta, P. K.; Major, D. T. Benchmarking the Ability of Common Docking Programs to Correctly Reproduce and Score Binding Modes in SARS-CoV-2 Protease Mpro. *J. Chem. Inf. Model.* **2021**, *61* (6), 2957−2966.
(43) Sztain, T.; Amaro, R.; McCammon, J. A. Elucidation of Cryptic and Allosteric Pockets within the SARS-CoV-2 Main Protease. *J. Chem. Inf. Model.* **2021**, *61* (7), 3495−3501.
(44) Jaffrelot Inizan, T.; Célerse, F.; Adjoua, O.; El Ahdab, D.; Jolly, L.-H.; Liu, C.; Ren, P.; Montes, M.; Lagarde, N.; Lagardère, L.; Monmarché, P.; Piquemal, J.-P. High-Resolution Mining of the SARS-CoV-2 Main Protease Conformational Space: Supercomputer-Driven Unsupervised Adaptive Sampling. *Chem. Sci.* **2021**, *12* (13), 4889−4907.
(45) Moghadasi, S. A.; Heilmann, E.; Khalil, A. M.; Nnabuife, C.; Kearns, F. L.; Ye, C.; Moraes, S. N.; Costacurta, F.; Esler, M. A.; Aihara, H.; Von Laer, D.; Martinez-Sobrido, L.; Palzkill, T.; Amaro, R. E.; Harris, R. S. Transmissible SARS-CoV-2 Variants with Resistance to Clinical Protease Inhibitors. *Sci. Adv.* **2023**, *9* (13), No. eade8778.
(46) Chan, H. T. H.; Oliveira, A. S. F.; Schofield, C. J.; Mulholland, A. J.; Duarte, F. Dynamical Nonequilibrium Molecular Dynamics Simulations Identify Allosteric Sites and Positions Associated with Drug Resistance in the SARS-CoV-2 Main Protease. *JACS Au* **2023**, *3* (6), 1767−1774.
(47) Balega, B.; Beer, M.; Spencer, J.; Colombo, G.; Serapian, S. A.; Oliveira, A. S. F.; Mulholland, A. J. Dynamical Nonequilibrium Molecular Dynamics Simulations Reveal Allosteric Networks, Signal Transduction Mechanisms, and Sites Associated with Drug Resistance in Biomolecular Systems. *Mol. Phys.* **2024**, No. e2428350.
(48) Günther, S.; Reinke, P. Y. A.; Fernández-García, Y.; Lieske, J.; Lane, T. J.; Ginn, H. M.; Koua, F. H. M.; Ehrt, C.; Ewert, W.; Oberthuer, D.; Yefanov, O.; Meier, S.; Lorenzen, K.; Krichel, B.; Kopicki, J.-D.; Gelisio, L.; Brehm, W.; Dunkel, I.; Seychell, B.; Gieseler, H.; Norton-Baker, B.; Escudero-Pérez, B.; Domaracky, M.; Saouane, S.; Tolstikova, A.; White, T. A.; Hänle, A.; Groessler, M.; Fleckenstein, H.; Trost, F.; Galchenkova, M.; Gevorkov, Y.; Li, C.; Awel, S.; Peck, A.; Barthelmess, M.; Schlünzen, F.; Lourdu Xavier, P.; Werner, N.; Andaleeb, H.; Ullah, N.; Falke, S.; Srinivasan, V.; França, B. A.; Schwinzer, M.; Brognaro, H.; Rogers, C.; Melo, D.; Zaitseva-Doyle, J. J.; Knoska, J.; Peña-Murillo, G. E.; Mashhour, A. R.; Hennicke, V.; Fischer, P.; Hakanpää, J.; Meyer, J.; Gribbon, P.; Ellinger, B.; Kuzikov, M.; Wolf, M.; Beccari, A. R.; Bourenkov, G.; Von Stetten, D.; Pompidor, G.; Bento, I.; Panneerselvam, S.; Karpics, I.; Schneider, T. R.; Garcia-Alai, M. M.; Niebling, S.; Günther, C.; Schmidt, C.; Schubert, R.; Han, H.; Boger, J.; Monteiro, D. C. F.; Zhang, L.; Sun, X.; Pletzer-Zelgert, J.; Wollenhaupt, J.; Feiler, C. G.; Weiss, M. S.; Schulz, E.-C.; Mehrabi, P.; Karničar, K.; Usenik, A.; Loboda, J.; Tidow, H.; Chari, A.; Hilgenfeld, R.; Uetrecht, C.; Cox, R.; Zaliani, A.; Beck, T.; Rarey, M.; Günther, S.; Turk, D.; Hinrichs, W.; Chapman, H. N.; Pearson, A. R.; Betzel, C.; Meents, A. X-Ray Screening Identifies Active Site and Allosteric Inhibitors of SARS-CoV-2 Main Protease. *Science* **2021**, *372* (6542), 642−646.
(49) Ramos-Guzmán, C. A.; Andjelkovic, M.; Zinovjev, K.; Ruiz-Pernía, J. J.; Tuñón, I. The Impact of SARS-CoV-2 3CL Protease Mutations on Nirmatrelvir Inhibitory Efficiency. Computational Insights into Potential Resistance Mechanisms. *Chem. Sci.* **2023**, *14* (10), 2686−2697.
(50) Wrapp, D.; Wang, N.; Corbett, K. S.; Goldsmith, J. A.; Hsieh, C.-L.; Abiona, O.; Graham, B. S.; McLellan, J. S. Cryo-EM Structure of the 2019-nCoV Spike in the Prefusion Conformation. *Science* **2020**, *367* (6483), 1260−1263.
(51) Walls, A. C.; Park, Y.-J.; Tortorici, M. A.; Wall, A.; McGuire, A. T.; Veesler, D. Structure, Function, and Antigenicity of the SARS-CoV-2 Spike Glycoprotein. *Cell* **2020**, *181* (2), 281.
(52) Hsieh, C.-L.; Goldsmith, J. A.; Schaub, J. M.; DiVenere, A. M.; Kuo, H.-C.; Javanmardi, K.; Le, K. C.; Wrapp, D.; Lee, A. G.; Liu, Y.; Chou, C.-W.; Byrne, P. O.; Hjorth, C. K.; Johnson, N. V.; Ludes-Meyers, J.; Nguyen, A. W.; Park, J.; Wang, N.; Amengor, D.; Lavinder, J. J.; Ippolito, G. C.; Maynard, J. A.; Finkelstein, I. J.; McLellan, J. S. Structure-Based Design of Prefusion-Stabilized SARS-CoV-2 Spikes. *Science* **2020**, *369* (6510), 1501−1505.
(53) Watanabe, Y.; Allen, J. D.; Wrapp, D.; McLellan, J. S.; Crispin, M. Site-Specific Glycan Analysis of the SARS-CoV-2 Spike. *Science* **2020**, *369* (6501), 330−333.
(54) Casalino, L.; Gaieb, Z.; Goldsmith, J. A.; Hjorth, C. K.; Dommer, A. C.; Harbison, A. M.; Fogarty, C. A.; Barros, E. P.; Taylor, B. C.; McLellan, J. S.; Fadda, E.; Amaro, R. E. Beyond Shielding: The Roles of Glycans in the SARS-CoV-2 Spike Protein. *ACS Cent. Sci.* **2020**, *6* (10), 1722−1734.
(55) Souza, P. F. N.; Mesquita, F. P.; Amaral, J. L.; Landim, P. G. C.; Lima, K. R. P.; Costa, M. B.; Farias, I. R.; Belém, M. O.; Pinto, Y. O.; Moreira, H. H. T.; Magalhaes, I. C. L.; Castelo-Branco, D. S. C. M.; Montenegro, R. C.; De Andrade, C. R. The Spike Glycoprotein of SARS-CoV-2: A Review of How Mutations of Spike Glycoproteins Have Driven the Emergence of Variants with High Transmissibility and Immune Escape. *Int. J. Biol. Macromol.* **2022**, *208*, 105−125.
(56) Andreano, E.; Piccini, G.; Licastro, D.; Casalino, L.; Johnson, N. V.; Paciello, I.; Dal Monego, S.; Pantano, E.; Manganaro, N.; Manenti, A.; Manna, R.; Casa, E.; Hyseni, I.; Benincasa, L.; Montomoli, E.; Amaro, R. E.; McLellan, J. S.; Rappuoli, R. SARS-CoV-2 Escape from a

https://doi.org/10.1021/acs.jpclett.4c03654
J. Phys. Chem. Lett. 2025, 16, 3249−3263

Highly Neutralizing COVID-19 Convalescent Plasma. *Proc. Natl. Acad. Sci. U. S. A.* **2021**, *118* (36), No. e2103154118.
(57) Ke, Z.; Oton, J.; Qu, K.; Cortese, M.; Zila, V.; McKeane, L.; Nakane, T.; Zivanov, J.; Neufeldt, C. J.; Cerikan, B.; Lu, J. M.; Peukes, J.; Xiong, X.; Kräusslich, H.-G.; Scheres, S. H. W.; Bartenschlager, R.; Briggs, J. A. G. Structures and Distributions of SARS-CoV-2 Spike Proteins on Intact Virions. *Nature* **2020**, *588* (7838), 498−502.
(58) Wormald, M. R.; Dwek, R. A. Glycoproteins: Glycan Presentation and Protein-Fold Stability. *Structure* **1999**, *7* (7), R155−R160.
(59) Woo, H.; Park, S.-J.; Choi, Y. K.; Park, T.; Tanveer, M.; Cao, Y.; Kern, N. R.; Lee, J.; Yeom, M. S.; Croll, T. I.; Seok, C.; Im, W. Developing a Fully Glycosylated Full-Length SARS-CoV-2 Spike Protein Model in a Viral Membrane. *J. Phys. Chem. B* **2020**, *124* (33), 7128−7137.
(60) Turoňová, B.; Sikora, M.; Schürmann, C.; Hagen, W. J. H.; Welsch, S.; Blanc, F. E. C.; Von Bülow, S.; Gecht, M.; Bagola, K.; Hörner, C.; Van Zandbergen, G.; Landry, J.; De Azevedo, N. T. D.; Mosalaganti, S.; Schwarz, A.; Covino, R.; Mühlebach, M. D.; Hummer, G.; Krijnse Locker, J.; Beck, M. In Situ Structural Analysis of SARS-CoV-2 Spike Reveals Flexibility Mediated by Three Hinges. *Science* **2020**, *370* (6513), 203−208.
(61) Shajahan, A.; Supekar, N. T.; Gleinich, A. S.; Azadi, P. Deducing the N- and O-Glycosylation Profile of the Spike Protein of Novel Coronavirus SARS-CoV-2. *Glycobiology* **2020**, *30* (12), 981−988.
(62) Grant, O. C.; Montgomery, D.; Ito, K.; Woods, R. J. Analysis of the SARS-CoV-2 Spike Protein Glycan Shield Reveals Implications for Immune Recognition. *Sci. Rep.* **2020**, *10* (1), 14991.
(63) Huber, G. A.; Kim, S. Weighted-Ensemble Brownian Dynamics Simulations for Protein Association Reactions. *Biophys. J.* **1996**, *70* (1), 97−110.
(64) Zuckerman, D. M.; Chong, L. T. Weighted Ensemble Simulation: Review of Methodology, Applications, and Software. *Annu. Rev. Biophys.* **2017**, *46* (1), 43−57.
(65) Sztain, T.; Ahn, S.-H.; Bogetti, A. T.; Casalino, L.; Goldsmith, J. A.; Seitz, E.; McCool, R. S.; Kearns, F. L.; Acosta-Reyes, F.; Maji, S.; Mashayekhi, G.; McCammon, J. A.; Ourmazd, A.; Frank, J.; McLellan, J. S.; Chong, L. T.; Amaro, R. E. A Glycan Gate Controls Opening of the SARS-CoV-2 Spike Protein. *Nat. Chem.* **2021**, *13* (10), 963−968.
(66) Harbison, A. M.; Fogarty, C. A.; Phung, T. K.; Satheesan, A.; Schulz, B. L.; Fadda, E. Fine-Tuning the Spike: Role of the Nature and Topology of the Glycan Shield in the Structure and Dynamics of the SARS-CoV-2 S. *Chem. Sci.* **2022**, *13* (2), 386−395.
(67) Cerutti, G.; Guo, Y.; Zhou, T.; Gorman, J.; Lee, M.; Rapp, M.; Reddem, E. R.; Yu, J.; Bahna, F.; Bimela, J.; Huang, Y.; Katsamba, P. S.; Liu, L.; Nair, M. S.; Rawi, R.; Olia, A. S.; Wang, P.; Zhang, B.; Chuang, G.-Y.; Ho, D. D.; Sheng, Z.; Kwong, P. D.; Shapiro, L. Potent SARS-CoV-2 Neutralizing Antibodies Directed against Spike N-Terminal Domain Target a Single Supersite. *Cell Host Microbe* **2021**, *29* (5), 819.
(68) Guseman, A. J.; Rennick, L. J.; Nambulli, S.; Roy, C. N.; Martinez, D. R.; Yang, D. T.; Bhinderwala, F.; Vergara, S.; Schaefer, A.; Baric, R. S.; Ambrose, Z.; Duprex, W. P.; Gronenborn, A. M. Targeting Spike Glycans to Inhibit SARS-CoV2 Viral Entry. *Proc. Natl. Acad. Sci. U. S. A.* **2023**, *120* (38), No. e2301518120.
(69) Kim, S. H.; Kearns, F. L.; Rosenfeld, M. A.; Casalino, L.; Papanikolas, M. J.; Simmerling, C.; Amaro, R. E.; Freeman, R. *GlycoGrip*: Cell Surface-Inspired Universal Sensor for Betacoronaviruses. *ACS Cent. Sci.* **2022**, *8* (1), 22−42.
(70) Kim, S. H.; Kearns, F. L.; Rosenfeld, M. A.; Votapka, L.; Casalino, L.; Papanikolas, M.; Amaro, R. E.; Freeman, R. SARS-CoV-2 Evolved Variants Optimize Binding to Cellular Glycocalyx. *Cell Rep. Phys. Sci.* **2023**, *4* (4), No. 101346.
(71) Paiardi, G.; Richter, S.; Oreste, P.; Urbinati, C.; Rusnati, M.; Wade, R. C. The Binding of Heparin to Spike Glycoprotein Inhibits SARS-CoV-2 Infection by Three Mechanisms. *J. Biol. Chem.* **2022**, *298* (2), No. 101507.
(72) Blazhynska, M.; Lagardère, L.; Liu, C.; Adjoua, O.; Ren, P.; Piquemal, J.-P. Water−Glycan Interactions Drive the SARS-CoV-2 Spike Dynamics: Insights into Glycan-Gate Control and Camouflage Mechanisms. *Chem. Sci.* **2024**, *15* (35), 14177−14187.
(73) Fallon, L.; Belfon, K. A. A.; Raguette, L.; Wang, Y.; Stepanenko, D.; Cuomo, A.; Guerra, J.; Budhan, S.; Varghese, S.; Corbo, C. P.; Rizzo, R. C.; Simmerling, C. Free Energy Landscapes from SARS-CoV-2 Spike Glycoprotein Simulations Suggest That RBD Opening Can Be Modulated via Interactions in an Allosteric Pocket. *J. Am. Chem. Soc.* **2021**, *143* (30), 11349−11360.
(74) Dokainish, H. M.; Re, S.; Mori, T.; Kobayashi, C.; Jung, J.; Sugita, Y. The Inherent Flexibility of Receptor Binding Domains in SARS-CoV-2 Spike Protein. *eLife* **2022**, *11*, No. e75720.
(75) Pang, Y. T.; Acharya, A.; Lynch, D. L.; Pavlova, A.; Gumbart, J. C. SARS-CoV-2 Spike Opening Dynamics and Energetics Reveal the Individual Roles of Glycans and Their Collective Impact. *Commun. Biol.* **2022**, *5* (1), 1170.
(76) Toelzer, C.; Gupta, K.; Yadav, S. K. N.; Borucu, U.; Davidson, A. D.; Kavanagh Williamson, M.; Shoemark, D. K.; Garzoni, F.; Staufer, O.; Milligan, R.; Capin, J.; Mulholland, A. J.; Spatz, J.; Fitzgerald, D.; Berger, I.; Schaffitzel, C. Free Fatty Acid Binding Pocket in the Locked Structure of SARS-CoV-2 Spike Protein. *Science* **2020**, *370* (6517), 725−730.
(77) Shoemark, D. K.; Colenso, C. K.; Toelzer, C.; Gupta, K.; Sessions, R. B.; Davidson, A. D.; Berger, I.; Schaffitzel, C.; Spencer, J.; Mulholland, A. J. Molecular Simulations Suggest Vitamins, Retinoids and Steroids as Ligands of the Free Fatty Acid Pocket of the SARS-CoV-2 Spike Protein**. *Angew. Chem., Int. Ed.* **2021**, *60* (13), 7098−7110.
(78) Staufer, O.; Gupta, K.; Hernandez Bücher, J. E.; Kohler, F.; Sigl, C.; Singh, G.; Vasileiou, K.; Yagüe Relimpio, A.; Macher, M.; Fabritz, S.; Dietz, H.; Cavalcanti Adam, E. A.; Schaffitzel, C.; Ruggieri, A.; Platzman, I.; Berger, I.; Spatz, J. P. Synthetic Virions Reveal Fatty Acid-Coupled Adaptive Immunogenicity of SARS-CoV-2 Spike Glycoprotein. *Nat. Commun.* **2022**, *13* (1), 868.
(79) Gupta, K.; Toelzer, C.; Williamson, M. K.; Shoemark, D. K.; Oliveira, A. S. F.; Matthews, D. A.; Almuqrin, A.; Staufer, O.; Yadav, S. K. N.; Borucu, U.; Garzoni, F.; Fitzgerald, D.; Spatz, J.; Mulholland, A. J.; Davidson, A. D.; Schaffitzel, C.; Berger, I. Structural Insights in Cell-Type Specific Evolution of Intra-Host Diversity by SARS-CoV-2. *Nat. Commun.* **2022**, *13* (1), 222.
(80) Oliveira, S. F.; Shoemark, D. K.; Avila Ibarra, A.; Davidson, A. D.; Berger, I.; Schaffitzel, C.; Mulholland, A. J. The Fatty Acid Site Is Coupled to Functional Motifs in the SARS-CoV-2 Spike Protein and Modulates Spike Allosteric Behaviour. *Comput. Struct. Biotechnol. J.* **2022**, *20*, 139−147.
(81) Oliveira, A. S. F.; Kearns, F. L.; Rosenfeld, M. A.; Casalino, L.; Berger, I.; Schaffitzel, C.; Davidson, A. D.; Amaro, R. E.; Mulholland, A. J. Allosteric Modulation by the Fatty Acid Site in the Glycosylated SARS-CoV-2 Spike. *eLife* **2024**, *13*, RP97313.
(82) Oliveira, A. S. F.; Shoemark, D. K.; Davidson, A. D.; Berger, I.; Schaffitzel, C.; Mulholland, A. J. SARS-CoV-2 Spike Variants Differ in Their Allosteric Responses to Linoleic Acid. *J. Mol. Cell Biol.* **2023**, *15* (3), mjad021.
(83) Freeman, S. L.; Oliveira, A. S. F.; Gallio, A. E.; Rosa, A.; Simitakou, M. K.; Arthur, C. J.; Mulholland, A. J.; Cherepanov, P.; Raven, E. L. Heme Binding to the SARS-CoV-2 Spike Glycoprotein. *J. Biol. Chem.* **2023**, *299* (8), No. 105014.
(84) Oliveira, A. S. F.; Ibarra, A. A.; Bermudez, I.; Casalino, L.; Gaieb, Z.; Shoemark, D. K.; Gallagher, T.; Sessions, R. B.; Amaro, R. E.; Mulholland, A. J. A Potential Interaction between the SARS-CoV-2 Spike Protein and Nicotinic Acetylcholine Receptors. *Biophys. J.* **2021**, *120* (6), 983−993.
(85) Changeux, J.-P.; Amoura, Z.; Rey, F. A.; Miyara, M. A Nicotinic Hypothesis for Covid-19 with Preventive and Therapeutic Implications. *C. R. Biol.* **2020**, *343* (1), 33−39.
(86) O'Brien, B. C. V.; Weber, L.; Hueffer, K.; Weltzin, M. M. SARS-CoV-2 Spike Ectodomain Targets A7 Nicotinic Acetylcholine Receptors. *J. Biol. Chem.* **2023**, *299* (5), No. 104707.
(87) Cheng, M. H.; Zhang, S.; Porritt, R. A.; Noval Rivas, M.; Paschold, L.; Willscher, E.; Binder, M.; Arditi, M.; Bahar, I.

https://doi.org/10.1021/acs.jpclett.4c03654
J. Phys. Chem. Lett. 2025, 16, 3249−3263

Superantigenic Character of an Insert Unique to SARS-CoV-2 Spike Supported by Skewed TCR Repertoire in Patients with Hyperinflammation. *Proc. Natl. Acad. Sci. U. S. A.* **2020**, *117* (41), 25254−25262.
(88) Barros, E. P.; Casalino, L.; Gaieb, Z.; Dommer, A. C.; Wang, Y.; Fallon, L.; Raguette, L.; Belfon, K.; Simmerling, C.; Amaro, R. E. The Flexibility of ACE2 in the Context of SARS-CoV-2 Infection. *Biophys. J.* **2021**, *120* (6), 1072−1084.
(89) Mehdipour, A. R.; Hummer, G. Dual Nature of Human ACE2 Glycosylation in Binding to SARS-CoV-2 Spike. *Proc. Natl. Acad. Sci. U. S. A.* **2021**, *118* (19), No. e2100425118.
(90) Spinello, A.; Saltalamacchia, A.; Magistrato, A. Is the Rigidity of SARS-CoV-2 Spike Receptor-Binding Motif the Hallmark for Its Enhanced Infectivity? Insights from All-Atom Simulations. *J. Phys. Chem. Lett.* **2020**, *11* (12), 4785−4790.
(91) Mugnai, M. L.; Thirumalai, D. Allosteric Communication between ACE2 Active Site and Binding Interface with SARS-CoV-2. *J. Chem. Phys.* **2023**, *158* (21), No. 215102.
(92) Mugnai, M. L.; Shin, S.; Thirumalai, D. Entropic Contribution of ACE2 Glycans to RBD Binding. *Biophys. J.* **2023**, *122* (12), 2506−2517.
(93) Zhao, P.; Praissman, J. L.; Grant, O. C.; Cai, Y.; Xiao, T.; Rosenbalm, K. E.; Aoki, K.; Kellman, B. P.; Bridger, R.; Barouch, D. H.; Brindley, M. A.; Lewis, N. E.; Tiemeyer, M.; Chen, B.; Woods, R. J.; Wells, L. Virus-Receptor Interactions of Glycosylated SARS-CoV-2 Spike and Human ACE2 Receptor. *Cell Host Microbe* **2020**, *28* (4), 586.
(94) Casalino, L.; Dommer, A. C.; Gaieb, Z.; Barros, E. P.; Sztain, T.; Ahn, S.-H.; Trifan, A.; Brace, A.; Bogetti, A. T.; Clyde, A.; Ma, H.; Lee, H.; Turilli, M.; Khalid, S.; Chong, L. T.; Simmerling, C.; Hardy, D. J.; Maia, J. D.; Phillips, J. C.; Kurth, T.; Stern, A. C.; Huang, L.; McCalpin, J. D.; Tatineni, M.; Gibbs, T.; Stone, J. E.; Jha, S.; Ramanathan, A.; Amaro, R. E. AI-Driven Multiscale Simulations Illuminate Mechanisms of SARS-CoV-2 Spike Dynamics. *Int. J. High Perform. Comput. Appl.* **2021**, *35* (5), 432−451.
(95) Spinello, A.; Saltalamacchia, A.; Borišek, J.; Magistrato, A. Allosteric Cross-Talk among Spike's Receptor-Binding Domain Mutations of the SARS-CoV-2 South African Variant Triggers an Effective Hijacking of Human Cell Receptor. *J. Phys. Chem. Lett.* **2021**, *12* (25), 5987−5993.
(96) Jawad, B.; Adhikari, P.; Podgornik, R.; Ching, W.-Y. Key Interacting Residues between RBD of SARS-CoV-2 and ACE2 Receptor: Combination of Molecular Dynamics Simulation and Density Functional Calculation. *J. Chem. Inf. Model.* **2021**, *61* (9), 4425−4441.
(97) Wang, D.; Zhang, Z.; Baudys, J.; Haynes, C.; Osman, S. H.; Zhou, B.; Barr, J. R.; Gumbart, J. C. Enhanced Surface Accessibility of SARS-CoV-2 Omicron Spike Protein Due to an Altered Glycosylation Profile. *ACS Infect. Dis.* **2024**, *10* (6), 2032−2046.
(98) Ives, C. M.; Nguyen, L.; Fogarty, C. A.; Harbison, A. M.; Durocher, Y.; Klassen, J.; Fadda, E. Role of N343 Glycosylation on the SARS-CoV-2 S RBD Structure and Co-Receptor Binding across Variants of Concern. *eLife* **2024**, *13*, No. RP95708.
(99) Triveri, A.; Serapian, S. A.; Marchetti, F.; Doria, F.; Pavoni, S.; Cinquini, F.; Moroni, E.; Rasola, A.; Frigerio, F.; Colombo, G. SARS-CoV-2 Spike Protein Mutations and Escape from Antibodies: A Computational Model of Epitope Loss in Variants of Concern. *J. Chem. Inf. Model.* **2021**, *61* (9), 4687−4700.
(100) Triveri, A.; Casali, E.; Frasnetti, E.; Doria, F.; Frigerio, F.; Cinquini, F.; Pavoni, S.; Moroni, E.; Marchetti, F.; Serapian, S. A.; Colombo, G. Conformational Behavior of SARS-Cov-2 Spike Protein Variants: Evolutionary Jumps in Sequence Reverberate in Structural Dynamic Differences. *J. Chem. Theory Comput.* **2023**, *19* (7), 2120−2134.
(101) Sikora, M.; Von Bülow, S.; Blanc, F. E. C.; Gecht, M.; Covino, R.; Hummer, G. Computational Epitope Map of SARS-CoV-2 Spike Protein. *PLOS Comput. Biol.* **2021**, *17* (4), No. e1008790.
(102) Serapian, S. A.; Marchetti, F.; Triveri, A.; Morra, G.; Meli, M.; Moroni, E.; Sautto, G. A.; Rasola, A.; Colombo, G. The Answer Lies in the Energy: How Simple Atomistic Molecular Dynamics Simulations May Hold the Key to Epitope Prediction on the Fully Glycosylated SARS-CoV-2 Spike Protein. *J. Phys. Chem. Lett.* **2020**, *11* (19), 8084−8093.
(103) Buzas, D.; Bunzel, A. H.; Staufer, O.; Milodowski, E. J.; Edmunds, G. L.; Bufton, J. C.; Vidana Mateo, B. V.; Yadav, S. K. N.; Gupta, K.; Fletcher, C.; Williamson, M. K.; Harrison, A.; Borucu, U.; Capin, J.; Francis, O.; Balchin, G.; Hall, S.; Vega, M. V.; Durbesson, F.; Lingappa, S.; Vincentelli, R.; Roe, J.; Wooldridge, L.; Burt, R.; Anderson, R. J. L.; Mulholland, A. J.; Bristol Uncover Group; Hare, J.; Bailey, M.; Davidson, A. D.; Finn, A.; Morgan, D.; Mann, J.; Spatz, J.; Garzoni, F.; Schaffitzel, C.; Berger, I. *In Vitro* Generated Antibodies Guide Thermostable ADDomer Nanoparticle Design for Nasal Vaccination and Passive Immunization against SARS-CoV-2. *Antib. Ther.* **2023**, *6* (4), 277−297.
(104) Dodero-Rojas, E.; Onuchic, J. N.; Whitford, P. C. Sterically Confined Rearrangements of SARS-CoV-2 Spike Protein Control Cell Invasion. *eLife* **2021**, *10*, No. e70362.
(105) Clementi, C.; Nymeyer, H.; Onuchic, J. N. Topological and Energetic Factors: What Determines the Structural Details of the Transition State Ensemble and "En-Route" Intermediates for Protein Folding? An Investigation for Small Globular Proteins. *J. Mol. Biol.* **2000**, *298* (5), 937−953.
(106) Clementi, C.; García, A. E.; Onuchic, J. N. Interplay Among Tertiary Contacts, Secondary Structure Formation and Side-Chain Packing in the Protein Folding Mechanism: All-Atom Representation Study of Protein L. *J. Mol. Biol.* **2003**, *326* (3), 933−954.
(107) Nuqui, X.; Casalino, L.; Zhou, L.; Shehata, M.; Wang, A.; Tse, A. L.; Ojha, A. A.; Kearns, F. L.; Rosenfeld, M. A.; Miller, E. H.; Acreman, C. M.; Ahn, S.-H.; Chandran, K.; McLellan, J. S.; Amaro, R. E. Simulation-Driven Design of Stabilized SARS-CoV-2 Spike S2 Immunogens. *Nat. Commun.* **2024**, *15* (1), 7370.
(108) Kapoor, K.; Chen, T.; Tajkhorshid, E. Posttranslational Modifications Optimize the Ability of SARS-CoV-2 Spike for Effective Interaction with Host Cell Receptors. *Proc. Natl. Acad. Sci. U. S. A.* **2022**, *119* (28), No. e2119761119.
(109) Dommer, A.; Casalino, L.; Kearns, F.; Rosenfeld, M.; Wauer, N.; Ahn, S.-H.; Russo, J.; Oliveira, S.; Morris, C.; Bogetti, A.; Trifan, A.; Brace, A.; Sztain, T.; Clyde, A.; Ma, H.; Chennubhotla, C.; Lee, H.; Turilli, M.; Khalid, S.; Tamayo-Mendoza, T.; Welborn, M.; Christensen, A.; Smith, D. G.; Qiao, Z.; Sirumalla, S. K.; O'Connor, M.; Manby, F.; Anandkumar, A.; Hardy, D.; Phillips, J.; Stern, A.; Romero, J.; Clark, D.; Dorrell, M.; Maiden, T.; Huang, L.; McCalpin, J.; Woods, C.; Gray, A.; Williams, M.; Barker, B.; Rajapaksha, H.; Pitts, R.; Gibbs, T.; Stone, J.; Zuckerman, D. M.; Mulholland, A. J.; Miller, T.; Jha, S.; Ramanathan, A.; Chong, L.; Amaro, R. E. #COVIDisAirborne: AI-Enabled Multiscale Computational Microscopy of Delta SARS-CoV-2 in a Respiratory Aerosol. *Int. J. High Perform. Comput. Appl.* **2023**, *37* (1), 28−44.
(110) Lee, H.; Turilli, M.; Jha, S.; Bhowmik, D.; Ma, H.; Ramanathan, A. DeepDriveMD: Deep-Learning Driven Adaptive Molecular Simulations for Protein Folding. In *2019 IEEE/ACM Third Workshop on Deep Learning on Supercomputers (DLS)*; IEEE: 2019; pp 12−19. DOI: 10.1109/DLS49591.2019.00007.
(111) Qiao, Z.; Welborn, M.; Anandkumar, A.; Manby, F. R.; Miller, T. F. OrbNet: Deep Learning for Quantum Chemistry Using Symmetry-Adapted Atomic-Orbital Features. *J. Chem. Phys.* **2020**, *153* (12), No. 124111.
(112) Amaro, R.; Åqvist, J.; Bahar, I.; Battistini, F.; Bellaiche, A.; Beltran, D.; Biggin, P. C.; Bonomi, M.; Bowman, G. R.; Bryce, R.; Bussi, G.; Carloni, P.; Case, D.; Cavalli, A.; Chang, C.-E. A.; III, T. E. C.; Cheung, M. S.; Chipot, C.; Chong, L. T.; Choudhary, P.; Cisneros, G. A.; Clementi, C.; Collepardo-Guevara, R.; Coveney, P.; Covino, R.; Crawford, T. D.; Peraro, M. D.; de Groot, B.; Delemotte, L.; Vivo, M. D.; Essex, J.; Fraternali, F.; Gao, J.; Gelpí, J. L.; Gervasio, F. L.; Gonzalez-Nilo, F. D.; Grubmüller, H.; Guenza, M.; Guzman, H. V.; Harris, S.; Head-Gordon, T.; Hernandez, R.; Hospital, A.; Huang, N.; Huang, X.; Hummer, G.; Iglesias-Fernández, J.; Jensen, J. H.; Jha, S.; Jiao, W.; Jorgensen, W. L.; Kamerlin, S. C. L.; Khalid, S.; Laughton, C.; Levitt, M.; Limongelli, V.; Lindahl, E.; Lindorff-Larsen, K.; Loverde, S.;

https://doi.org/10.1021/acs.jpclett.4c03654
J. Phys. Chem. Lett. 2025, 16, 3249−3263

Lundborg, M.; Luo, Y. L.; Luque, F. J.; Lynch, C. I.; MacKerell, A.; Magistrato, A.; Marrink, S. J.; Martin, H.; McCammon, J. A.; Merz, K.; Moliner, V.; Mulholland, A.; Murad, S.; Naganathan, A. N.; Nangia, S.; Noe, F.; Noy, A.; Oláh, J.; O'Mara, M.; Ondrechen, M. J.; Onuchic, J. N.; Onufriev, A.; Osuna, S.; Panchenko, A. R.; Pantano, S.; Parish, C.; Parrinello, M.; Perez, A.; Perez-Acle, T.; Perilla, J. R.; Pettitt, B. M.; Pietropalo, A.; Piquemal, J.-P.; Poma, A.; Praprotnik, M.; Ramos, M. J.; Ren, P.; Reuter, N.; Roitberg, A.; Rosta, E.; Rovira, C.; Roux, B.; Röthlisberger, U.; Sanbonmatsu, K. Y.; Schlick, T.; Shaytan, A. K.; Simmerling, C.; Smith, J. C.; Sugita, Y.; Świderek, K.; Taiji, M.; Tao, P.; Tikhonova, I. G.; Tirado-Rives, J.; Tunón, I.; Kamp, M. W. V. D.; der Spoel, D. V.; Velankar, S.; Voth, G. A.; Wade, R.; Warshel, A.; Welborn, V. V.; Wetmore, S.; Wong, C. F.; Yang, L.-W.; Zacharias, M.; Orozco, M. The Need to Implement FAIR Principles in Biomolecular Simulations. arXiv August 30, 2024. DOI: 10.48550/arXiv.2407.16584.

(113) National Data Platform. https://nationaldataplatform.org/ (accessed 2024-12-11).

(114) MDDB, Molecular Dynamics Data Bank. https://mddbr.eu/ (accessed 2024-11-12).

https://doi.org/10.1021/acs.jpclett.4c03654
J. Phys. Chem. Lett. 2025, 16, 3249−3263